



HAL
open science

Bioconcentration, bioaccumulation and biomagnification of mercury in plankton of the Mediterranean Sea

Javier Angel Tesán-Onrubia, Lars-Eric Heimbürger-Boavida, Aurélie Dufour,
Mireille Harmelin-Vivien, Isabel García-Arévalo, Joël Knoery, Bastien
Thomas, François Carlotti, Marc Tedetti, Daniela Bănaru

► **To cite this version:**

Javier Angel Tesán-Onrubia, Lars-Eric Heimbürger-Boavida, Aurélie Dufour, Mireille Harmelin-Vivien, Isabel García-Arévalo, et al.. Bioconcentration, bioaccumulation and biomagnification of mercury in plankton of the Mediterranean Sea. *Marine Pollution Bulletin*, 2023, 194, pp.115439. 10.1016/j.marpolbul.2023.115439 . hal-04192423

HAL Id: hal-04192423

<https://amu.hal.science/hal-04192423>

Submitted on 31 Aug 2023

HAL is a multi-disciplinary open access archive for the deposit and dissemination of scientific research documents, whether they are published or not. The documents may come from teaching and research institutions in France or abroad, or from public or private research centers.

L'archive ouverte pluridisciplinaire **HAL**, est destinée au dépôt et à la diffusion de documents scientifiques de niveau recherche, publiés ou non, émanant des établissements d'enseignement et de recherche français ou étrangers, des laboratoires publics ou privés.

1 **Bioconcentration, bioaccumulation and biomagnification of mercury in plankton of the**
2 **Mediterranean Sea**

3 Javier Angel Tesán-Onrubia^{a*}, Lars-Eric Heimbürger-Boavida^a, Aurélie Dufour^a, Mireille
4 Harmelin-Vivien^a, Isabel García-Arévalo^b, Joël Knoery^b, Bastien Thomas^b, François
5 Carlotti^a, Marc Tedetti^a, Daniela Bănar^{a*}

6 ^aAix Marseille Univ, Université de Toulon, CNRS, IRD, MIO UMI110, Marseille, France

7 ^bIfremer, CCEM Contamination Chimique des Ecosystèmes Marins, F-44311 Nantes,
8 France

9
10 * Correspondence:

11 Javier Angel Tesán-Onrubia; javier.tesan@mio.osupytheas.fr

12 Daniela Bănar; daniela.banaru@mio.osupytheas.fr

13 Lars-Eric Heimbürger-Boavida; lars-eric.heimburger@mio.osupytheas.fr

14
15 For submission to Marine Pollution Bulletin – Special issue “Plankton and Contaminants in
16 the Mediterranean Sea: Biological pump and interactions from regional to global
17 approaches”

18
19 **Revised version**

20
21 **Highlights**

- 22 - Highest THg bioconcentration was highlighted in picoplankton
- 23 - MMHg biomagnified while THg decreased along the plankton food web
- 24 - MMHg bioaccumulated and biomagnified in zooplankton
- 25 - Highest zooplankton MMHg concentrations were observed in oligotrophic areas

26
27 **Abstract**

28
29 Plankton plays a prominent role in the bioaccumulation of mercury (Hg). The MERITE-
30 HIPPOCAMPE campaign was carried out in spring 2019 along a north-south transect
31 including coastal and offshore areas of the Mediterranean Sea. Sampling of sea water and
32 plankton by pumping and nets was carried out in the chlorophyll maximum layer. Two size-
33 fractions of phytoplankton (0.7–2.7 and 2.7–20 µm) and five of zooplankton (between 60

1 34 and >2000 μm) were separated, and their total mercury (THg) and monomethylmercury
2 35 (MMHg) contents were measured. Bioconcentration of THg was significantly higher in the
3 36 smallest phytoplankton size-fraction dominated by *Synechococcus* spp. The bioaccumulation
4 37 and biomagnification of MMHg in zooplankton was influenced by size, food sources,
5 38 biochemical composition and trophic level. MMHg was biomagnified in the plankton food
6 39 web, while THg decreased toward higher trophic levels. Higher MMHg concentrations were
7 40 measured in oligotrophic areas. Plankton communities in the Southern Mediterranean Sea
8 41 had lower MMHg concentrations than those in the Northern Mediterranean Sea. These
9 42 results highlighted the influence of environmental conditions and trophodynamics on the
10 43 transfer of Hg in Mediterranean plankton food webs, with implications for higher trophic
11 44 level consumers.
12
13
14
15
16
17
18
19
20
21

22

23 46 **Keywords**

24 47 Mercury, methylmercury, plankton, trophic transfer, contamination, food web
25
26

27

28 49 **1. Introduction**

29 50

30 51 Mercury (Hg), predominantly in its inorganic form, is released to the atmosphere and the
31 52 ocean from natural and anthropogenic sources, with the latter largely outweighing the
32 53 former (Outridge et al., 2018). Anthropogenic Hg emissions are thought to have tripled
33 54 surface ocean Hg levels (Lamborg et al., 2014). Marine apex predator Hg levels are driven
34 55 by anthropogenic Hg inputs and marine methylmercury (MeHg) production (Medieu et al.
35 56 2022), yet their relative importance is still poorly constrained (Wang et al. 2019). The
36 57 relatively small and semi-enclosed Mediterranean Sea receives proportionally more Hg and
37 58 the sea water MeHg dynamics are well known, making it an ideal case study (Cossa et al.,
38 59 2022). Microorganisms present in the ocean can convert inorganic Hg into MeHg species
39 60 (Villar et al., 2020), namely monomethylmercury (MMHg) and dimethylmercury (DMHg).
40 61 MMHg is a potent neurotoxic which bioaccumulates in organisms with size and age and
41 62 biomagnifies in food webs, reaching high concentrations in apex predators (Morel et al.,
42 63 1998). Mediterranean human populations are exposed to high levels of Hg related to higher
43 64 marine fish consumption, posing a potential health risk (UNEP, 2019; Petrova et al., 2020).
44 65 This is further exacerbated by the higher fish Hg levels in the Mediterranean Sea, often
45 66 exceeding regulatory limits (Aston and Fowler, 1985; Storelli and Marcotrigiano, 2001;
46
47
48
49
50
51
52
53
54
55
56
57
58
59
60
61
62
63
64
65

67 Tseng et al., 2021).

68 Several hypotheses have been proposed to explain the so-called “Mediterranean Hg
69 anomaly” (Aston and Fowler, 1985; Cossa and Coquery, 2005), mainly attributing the
70 higher biota Hg levels to enhanced MeHg production. The high methylation capacities
71 reported in the Mediterranean Sea may enhance MMHg availability to the lower trophic
72 levels, namely plankton (Cossa and Coquery, 2005, Monperrus et al., 2007; Cossa et al.,
73 2022). Similarly to the Arctic Ocean, the Mediterranean MeHg maxima are located at
74 shallow depths in proximity to the phytoplankton habitat, allowing for an efficient uptake
75 into the food web (Heimbürger et al., 2010, 2015; Cossa et al., 2012). Nevertheless, sea
76 water Hg concentrations alone cannot explain the “Mediterranean Hg anomaly” observed for
77 biota (Aston and Fowler, 1985; Cossa and Coquery, 2005). While Hg concentrations have
78 been extensively observed in Mediterranean higher trophic level biota (Cinnirella et al.,
79 2019 and references therein), only few studies have been conducted on plankton Hg levels
80 (Cossa et al., 2012; Chouvelon et al., 2019).

81 Although studies are scarce, plankton organisms are hypothesized to play a key role in the
82 accumulation and transfer of Hg in the Mediterranean food webs (Cossa and Coquery, 2005;
83 Harmelin-Vivien et al., 2009; Chouvelon et al., 2018, 2019; Cossa et al., 2022).
84 Phytoplankton bioconcentrates Hg more than 10,000 times from sea water, which is by far
85 the largest enrichment step of Hg along the marine food web (Lee and Fisher, 2016).
86 Mercury bioconcentration has been shown to be related to species and size, with the highest
87 bioconcentration for smallest phytoplankton cells largely driven by their higher surface-to-
88 volume ratio (Lee and Fisher, 2016). In the Mediterranean Sea, phytoplankton is mainly
89 composed of small cells (pico- and nanoplankton) with a low biomass (Leblanc et al., 2018;
90 Boudriga et al., 2022; Tesán-Onrubia et al., 2023), and a high Hg bioconcentration may thus
91 be expected (Chouvelon et al., 2018). In addition, the slow-sinking pico- and
92 nanophytoplankton cells are more prone to remineralization (Guidi et al., 2009) and thus to
93 providing more Hg for methylation (Heimbürger et al., 2010). Due to technical difficulties,
94 data on Hg concentrations in small phytoplankton fractions collected in the field remain
95 scarce to date (Gosnell and Mason, 2015; Gosnell et al., 2017). Zooplankton represents the
96 link between phytoplankton and higher trophic levels. MMHg bioaccumulates in
97 zooplankton with size and age mainly because of food uptake (Tsui and Wang, 2004;
98 Hammerschmidt et al., 2013). A size-based approach has become widely used to study the
99 structure and functioning of the planktonic compartment (Rau et al., 1990; Rolff, 2000;

100 Carlotti et al., 2008; Hunt et al., 2017). However, taxonomic and groups composition differ
101 between plankton size-fractions (Boudriga et al., 2023; Fierro-González et al., 2023).
102 Zooplankton may exhibit different feeding patterns across size-fractions, ranging from
103 herbivorous to carnivorous, resulting in different Hg exposure (Pućko et al., 2014).
104 Oligotrophic ecosystems are characterized by lower growth rates, which reduces the
105 biodilution of Hg in biota (i.e., decrease in Hg with increasing biomass) (Silva et al., 2008;
106 Cossa et al., 2012; Chauvelon et al., 2018). The relatively warm waters of the Mediterranean
107 Sea may stimulate Hg-methylating microbes (Bacci et al., 1989; Heimbürger et al. 2010),
108 likewise increase the metabolic activity of higher trophic levels, and reduce excretion rates
109 of MMHg (Remen et al., 2015; Maulvault et al., 2016). The biochemical composition of
110 organisms can influence their physico-chemical affinity for Hg bioaccumulation (Wu and
111 Wang, 2011; Charette et al., 2021). Overall, little is known about the biological mechanisms
112 of accumulation of Hg in plankton in the Mediterranean Sea and the influence of species,
113 size, and biochemical composition of plankton. Moreover, Hg biomagnification in the food
114 web may be related to food sources but also to trophic structure. The longer food web of
115 oligotrophic ecosystems (Décima, 2022; Tesán-Onrubia et al., 2023) may increase MMHg
116 biomagnification (Cossa et al., 2012, 2022). Nevertheless, to date, biomagnification in a
117 size-fractionated plankton food web has, to our knowledge, never been studied.
118 The Mediterranean Sea represents a semi-enclosed basin with spatial nutrient gradients and
119 different sources and concentrations of Hg in sea water (Durrieu de Madron et al., 2011;
120 Cossa et al., 2022). Spatial variations of Hg concentrations have been shown in both sea
121 water and sediments (Cossa and Martin, 1991; Horvat et al., 1999; Covelli et al., 2001;
122 Tessier et al., 2011; Rosati et al., 2020), potentially impacting Hg concentrations in fishes
123 (Kucuksezgin et al., 2001; Cresson et al., 2015) and at all levels of the food web (Chen et
124 al., 2008). Gosnell and Mason (2015) hypothesized that the spatial variability of Hg
125 concentrations in plankton size-fractions is also related to the plankton productivity.
126 However, in the Mediterranean Sea, no spatially resolved data is available on the Hg content
127 of plankton.
128 To investigate the “Mediterranean Hg anomaly” at the base of the pelagic food web,
129 sampling different plankton size classes remains a challenge, the main technical difficulty
130 being the collection of large quantities for subsequent chemical analyses. A key feature of
131 the MERITE-HIPPOCAMPE campaign was the implementation of targeted sampling
132 strategies for the collection of large quantities of size-fractionated phyto- and zooplankton at

133 the chlorophyll maximum layer (CML). Throughout the MERITE-HIPPOCAMPE cruise,
134 samples were taken for sea water, different size-fractions of phyto- (0.7–2.7, 2.7–20 μm)
135 and zooplankton (60–200, 200–500, 500–1000, 1000–2000 and $>2000 \mu\text{m}$). Complementary
136 studies were also conducted on environmental parameters, species or groups composition,
137 biochemical and stable isotopes composition of the different size-fractions (Boudriga et al.,
138 2022; Fierro-González et al., 2023; Tesán-Onrubia et al., 2023; Tedetti et al., 2023). The aim
139 of our study was to investigate the bioconcentration, bioaccumulation and biomagnification
140 of THg and MMHg in different plankton size classes in contrasted ecoregions of the
141 Mediterranean Sea.

143 2. Material and methods

145 2.1 Sampling preparation

147 The MERITE-HIPPOCAMPE cruise took place in the Mediterranean Sea, between April
148 13th and May 14th 2019, onboard the R/V *Antea* (Fig. 1; Tedetti and Tronczynski, 2019). A
149 total of 10 stations were sampled in different ecoregions, including coastal sites in the Bay
150 of Marseille and Toulon (France), in the Gulf of Gabès (Tunisia) and offshore
151 Mediterranean waters (Table S1). Details on the sampling sites, the hydro-bio-geochemical
152 context and the sampling techniques are reported in Tedetti et al. (2023).

153 Unfiltered sea water was collected under trace metal clean conditions with a 12 L GOFLO
154 bottle (General Oceanics). Sea water was filtered through a PFA filter holder (Savillex),
155 holding a 47 mm diameter glass fiber filter of 0.7 μm porosity (GF/F, Whatman), conserved
156 in PFA bottles and immediately analyzed. Suspended particulate matter was sampled using
157 McLane Large Volume Water Transfer System Samplers (WTS6-142LV, 4–8 L min^{-1}), also
158 called *in situ* pumps. These *in situ* pumps were mounted with bulk and sequential filtration
159 systems (Bishop et al., 2012), holding 142 mm diameter nylon (20 μm), GF/D (2.7 μm) and
160 GF/F (0.7 μm) filters, and typically filtered between 169 and 300 L. The glass fiber filters
161 (GF/D and GF/F, Whatman) were pre-combusted (450°C, 6 h), rinsed, dried and weighed
162 prior to deployment. The 20 μm nylon filters (Mougel, France) were cleaned (HCl 0.05%
163 v/v), dried and weighed prior to deployment. After deployment, the filters were stored
164 folded in half in pre-combusted aluminum foil at -20°C .

165 Zooplankton collection was carried out towing a Multinet Plankton Sampler (Midi type with

166 0.25 m² opening, Hydro-Bios) at ~2 knots. The obtained bulk sample was consecutively
167 sieved to obtain the following fractions: 60–200, 200–500, 500–1000, 1000–2000 and
168 >2000 µm. Samples were stored in cleaned polypropylene tubes and conserved frozen at –
169 20°C. In the laboratory, filters and zooplankton were freeze-dried before being analyzed.
170 Overall, 67 samples were collected for THg and MMHg measurements in different fractions.
171 We collected 10 samples of sea water, 10 samples of each of the following fractions: 0.7–
172 2.7, 2.7–20, 60–200, 200–500 µm, 9 samples of the 500–1000 µm fraction, 5 samples of the
173 1000–2000 µm fraction and 3 samples of the >2000 µm fraction.
174 Dry weight biomass and biochemical content of all the sieved size-fractions were analyzed
175 and are available in Tesán-Onrubia et al. (2023).

177 **2.2 Reagents and standards for Hg analyses**

179 Reagent and standard solutions were prepared in ultrapure water (18 MΩ cm; MilliQ).
180 Sodium tetraethylborate (Merseburger Spezialchemikalien) solution (1% m/v) was prepared
181 in ultrapure water and dispensed into 15 mL trace metal grade polypropylene vials (VWR).
182 The solution was frozen initially and, after thawing, stored at 4°C for up to 3 days. Sodium
183 acetate buffer solution (2 M) was prepared by diluting glacial acetic acid (J.T. Baker) and
184 anhydrous sodium acetate (J.T. Baker), which was muffled at 300°C for 3 h prior to making
185 up the solution. Nitric acid (14 M) and hydrochloric acid (12 M) were bi-distilled in a clean
186 room under trace metal free conditions.

187 Standard solutions of inorganic Hg (iHg) (0.9 µg L⁻¹) and MMHg (0.02 and 1 µg L⁻¹) for
188 plankton analysis were prepared from standard solutions (NIST3133 for iHg and a 1 µg L⁻¹
189 MMHg solution purchased from Brooks Rand Labs, traceable to NIST3133). The standards
190 were diluted in 0.5% v/v nitric acid and 0.2% v/v hydrochloric acid solution using a
191 precision balance (Mettler Toledo XS105; d = 0.01 mg).

193 **2.3 THg and MMHg in sea water**

195 Filtered dissolved total mercury (dHg) was analyzed on board by cold vapor atomic
196 fluorescence spectrometry (CV-AFS) immediately after sampling. The mineralization of all
197 dissolved Hg species was done using an acidic BrCl solution during 20 to 60 min prior to the
198 analyses. For shipboard analyses, we used a lab-built sample sparging device connected to a

199 Tekran 2500 fluorescence detector and a chromatography package to quantify fluorescence
200 peaks. For our analyses, a 40 mL aliquot of the digested sample containing its quantitatively
201 oxidized mercury (Hg^{2+}) was placed in a gas-stripping FEP tube. An excess of SnCl_2 was
202 added immediately before closing it to convert all Hg into gaseous elemental Hg, $\text{Hg}(0)$. The
203 sample was sparged in a FEP tube at 150 mL min^{-1} for 4 min with Hg-free Ar to exsolve
204 $\text{Hg}(0)$ and to sweep it toward a gold trap where it was retained. Mercury was thermally
205 desorbed from the trap and swept by an argon stream into the CV-AFS detector. For dHg
206 analyses, the daily 4-point external linear calibration curves were verified with an aliquot of
207 a certified reference material (ORMS-5, National Research Council Canada) that was
208 analyzed every fifth run. Additional 1-point recalibration curves were acquired when the
209 instrument's response drifts by more than 5% from the target value of the reference material.
210 Overall precision and accuracy of dHg measurements, based on repeated analyses of
211 samples, standards and CRMs, was better than 10%, and limits of quantification attained
212 during the cruise were better than 5 pg L^{-1} , based on repeated analyses of 4 pg Hg^{2+} .
213 Unfiltered MeHg species were analyzed back at the laboratory in samples acidified to 0.5%
214 v/v with HCl 11N, and stored in FEP bottles without headspace. Acidification converts the
215 gaseous DMHg to MMHg, and thus the sum of both is measured as MeHg. The general
216 principles of the hydride generation are as follows. Analyses were carried out by sparging a
217 40 mL sample aliquot with He while NaBH_4 was continuously added (10 g L^{-1} pumped at
218 0.25 mL min^{-1}). The evolved volatiles were retained on a 20 cm long, U-shaped cryogenic
219 trap and chromatography column (Chromosorb with silicone OV1 at 15%) immersed in
220 liquid nitrogen. When stripping of the MeHg is completed after 7 min, the trap is removed
221 from liquid nitrogen and heated. As it progressively warms, the trapped Hg species
222 including elemental and MeHg are released at different times from the column. Helium and
223 Hg gases exiting from the outlet of the column then flowed through a 20 cm x 1 mm inner
224 diameter quartz tube maintained at 800°C , where Hg species are pyrolyzed to elemental Hg.
225 The cooled helium and Hg vapor were then directed to a mirrored cell (Hellma, Germany) of
226 a CV-AFS detector (Tekran 2500).

227 A 2-point external calibration was done at the beginning of each day, and after every 5th
228 sample to account for potential instrumental drift. Based on the uncertainty of low amounts
229 of analyte (2 pg Hg as MMHg), the detection limit was 0.29 pg Hg as MMHg, in a 40 mL
230 sample (7 pg L^{-1}). The dissolved methylmercury (dMeHg) species were calculated by
231 subtracting the particulate (0.7 to $20 \text{ }\mu\text{m}$) from the unfiltered fraction.

232

233 2.4 THg and MMHg in plankton

234

235 THg was analyzed in zooplankton size-fractions ($>60 \mu\text{m}$) using atomic absorption
236 spectrometry (AAS, AMA 254, LECO). The analyzer was equipped with a low-level Hg
237 optical cell. The certified reference material (MESS-4, National Research Council Canada)
238 was measured at the beginning and end of the run to verify accuracy. The THg
239 measurements were always within the certified values and the limit of detection,
240 corresponding to the blank plus three times the standard deviation, was 23 pg.

241 In contrast to zooplankton, THg and MMHg on digested filters were simultaneously
242 measured by purge-and-trap gas chromatography pyrolysis atomic fluorescence
243 spectrometry (PT-GC-Pyr-AFS, MERX-M, Brooks Rand Labs) (Sharif et al., 2013). The
244 biomass collected on filters was too low for measuring THg in a subsample with a signal
245 close to the detection limits of the AAS. Secondly, particulate matter may not be evenly
246 distributed in the filters and may not be suitable for subsampling (Bishop et al., 2012).

247 Filters were digested, and both iHg and MMHg were derivatized and measured
248 simultaneously. Briefly, filters and zooplankton aliquots between 13 and 190 mg were
249 digested in 20 and 60 mL, pre-combusted (350°C , 5 h) glass vials with 4.57 M nitric acid
250 (3.5–15 mL) for 12 h at 60°C (Hammerschmidt and Fitzgerald, 2006). Amber glass vials (60
251 mL) were filled with ultrapure water and buffered with sodium acetate to pH 4.5–4.9. An
252 aliquot of the acidic extract (400–800 μL) was then added. The solution was spiked with iHg
253 (100 to 400 μL) and MMHg (10 to 400 μL) solutions for quantification *via* standard
254 addition.

255 Finally, we added the derivatizing agent, sodium tetraethylborate (NaBeT_4) and filled the
256 vial with ultrapure water until a slightly negative meniscus was formed. The cap was
257 tightened, and the preparation was gently mixed. The samples were measured by PT-GC-
258 Pyr-AFS. The chromatogram typically contains three peaks, corresponding to different
259 mercury species: elemental mercury (Hg^0), ethylmethylHg and diethylHg. THg was
260 calculated as the sum of iHg and MMHg. We followed a standard addition protocol to
261 estimate THg and MMHg concentrations. The low concentrations and matrix effect
262 associated with biological samples make standard addition a more reliable analytical
263 approach than external calibration. For a single sample, five measurements were performed
264 to construct a regression line. Of the five measurements, two corresponded to sample

265 replicates without addition, and the remaining three to three different volumes of standard
266 solution. The targeted standard volumes corresponded to between 1 and 5 times the amount
267 of iHg or MMHg present in the sample. The linear regression between added iHg or MMHg
268 and the peak height was calculated. The y-intercept of the linear regression was used to
269 obtain the iHg and MMHg concentrations. The correlation coefficients (R^2) ranged from
270 0.96 to 1.00. The certified reference material (DORM-4, National research council Canada)
271 was digested and measured similarly to the samples. The measurements corresponded
272 respectively to 79 and 85% of the THg and MMHg certified concentrations. The limits of
273 detection for iHg and MMHg were respectively 8 and 0.8 pg.

274 Based on the measurement made during the MERITE-HIPPOCAMPE cruise between
275 plankton biomass wet and dry weights (% of water in plankton: $90 \pm 3\%$; Tedetti et al.,
276 2023), a factor of 10 was used to allow comparison of the THg and MMHg concentrations
277 expressed here on a dry weight basis, with those reported in the literature. Further
278 experiments were carried out to assess the THg blanks in the filters, which could be due to
279 the retention of dissolved, colloidal and particulate Hg ($<0.7 \mu\text{m}$) (Table S2). Different
280 volumes of sea water (10–80 L) were filtered as replicates through three stacked $0.7 \mu\text{m}$
281 glass fiber filters (GF/F, 142 mm). THg blanks measured on the 2nd and 3rd filters were not
282 significantly different ($H = 1$; $p > 0.05$) and represented less than 2% of the particulate
283 fraction measured on the 1st filter ($n = 12$). We therefore assume that the THg measured on
284 the filters was representative of the particulate fraction, with a negligible contribution of the
285 dissolved ($<0.7 \mu\text{m}$) fraction.

287 2.5 Data treatment

289 The effect of size-fractions and geographical area on the THg, MMHg and fraction of
290 MMHg were assessed by means of one-way ANOVA (F) or non-parametric Kruskal-Wallis
291 (H) tests after testing for normality and homogeneity of variances, followed by appropriate
292 paired comparison tests, using the software Statistica 12. Principal component analysis
293 (PCA) was performed using the R software (R Core Team, 2017). The PCA used data from
294 Tesán-Onrubia et al. (2023) that may influence THg and MMHg in zooplankton: proteins,
295 carbohydrates, lipids, $\delta^{13}\text{C}$, $\delta^{15}\text{N}$, C/N, THg and MMHg in the 0.7–2.7 and 2.7–20 μm
296 fractions, phytoplankton size-fractions biomass, zooplankton size-fractions biomass, and
297 plankton group composition.

298 The bioconcentration factor of THg and MMHg (BCF_{Hg} , in $L\ kg^{-1}$) was calculated between
299 plankton and sea water:

$$BCF_{Hg} = \left(\frac{[Hg]_{Plankton}}{[Hg]_{Seawater}} \right) \times 10^6$$

300 where $[Hg]_{Plankton}$ is the dry weight concentrations of THg or MMHg on a given size-fraction
301 (in $ng\ g^{-1}$), $[Hg]_{sea\ water}$ is the dissolved concentrations of Hg (dHg) or MeHg (dMeHg) in sea
302 water (in $pg\ L^{-1}$), and 10^6 is the unit conversion factor.

303 The trophic magnification factor (TMF_{Hg}) of THg and MMHg was calculated within the
304 planktonic food web as follows:

$$TMF_{Hg} = 10^a$$

$$\text{Log } [Hg]_{Plankton} = \delta^{15}N * a + b$$

307 where $\log [Hg]_{Plankton}$ is the logarithm of the THg or MMHg concentration in plankton
308 fractions, $\delta^{15}N$ is the nitrogen stable isotope in the plankton fraction and a is the slope of the
309 linear regression.

3. Results and discussion

314 The basis of marine Mediterranean food webs is mainly constituted of pico- (0.7–2.7 μm) and
315 nanophytoplankton (2.7–20 μm) (Bănaru et al., 2013; 2019). These phytoplankton fractions
316 are consumed by zooplankton (Hunt et al., 2017; Tesán-Onrubia et al., 2023), which transfer
317 the organic matter and the associated contaminants up to higher trophic level consumers. THg
318 and MMHg measurements on the 0.7–2.7 and 2.7–20 μm size-fractions are scarce and were
319 usually only measured on relatively small sea water volumes (Gosnell and Mason, 2015;
320 Gosnell et al., 2017). In the present study, these analyses were performed on large volume
321 samples (>150 L), which enabled precise Hg species measurements and complementary
322 biological and biochemical analyses (Tesán-Onrubia et al., 2023).

3.1 THg and MMHg in phytoplankton

325 A contrasted pattern of the relationship between concentration and size was observed for THg
326 and MMHg in phyto- and zooplankton size classes (Fig. 2a, 2b, Tables S3, S4). Both THg and

327 MMHg concentrations decreased in phytoplankton with increasing cell size, but the difference
328 was statistically significant only for THg in the smallest size-fractions ($86 \pm 32 \text{ ng g}^{-1} \text{ dw}$ in
329 the $0.7\text{--}2.7 \mu\text{m}$ fraction, and $42 \pm 28 \text{ ng g}^{-1} \text{ dw}$ in the $2.7\text{--}20 \mu\text{m}$ fraction) ($F = 10.6$, $p =$
330 0.005). These values were in the upper range (maxima $42\text{--}160 \text{ ng g}^{-1} \text{ dw}$) of previous
331 observations obtained on a wide range of phytoplankton fractions (Baeyens et al., 2003;
332 Hammerschmidt and Fitzgerald, 2006; Beldożska and Kobos, 2018; Cossa et al., 2012;
333 Hammerschmidt et al., 2013; Gosnell and Mason, 2015; Lamborg et al., 2016; Fox et al.,
334 2017; Harding et al., 2018). However, our measurements were lower than the maxima (420--
335 $740 \text{ ng g}^{-1} \text{ dw}$) reported in studies with larger size-fractions (Bargagli et al., 1998), indirect
336 measurements (Luengen and Flegal, 2009), small volumes of filtered sea water (Gosnell et al.,
337 2017) and estuaries (Kehrig et al., 2009; Mason et al., 2021, 2023) (Table S5). Mean MMHg
338 concentrations of $1.2 \pm 0.7 \text{ ng g}^{-1} \text{ dw}$ and $0.8 \pm 0.6 \text{ ng g}^{-1} \text{ dw}$ were measured in the $0.7\text{--}2.7$
339 and in the $2.7\text{--}20 \mu\text{m}$ fractions, respectively, and are within the range of previous studies. Our
340 observations correspond well to MMHg concentration measured in phytoplankton (Baeyens et
341 al., 2003; Hammerschmidt and Fitzgerald, 2006; Luengen and Flegal 2009; Cossa et al., 2012;
342 Hammerschmidt et al., 2013; Gosnell and Mason, 2015; Gosnell et al., 2017; Fox et al., 2017;
343 Harding et al., 2018) but were lower than concentrations modeled for the Mediterranean Sea
344 ($2\text{--}15 \text{ ng g}^{-1} \text{ dw}$) (Rosati et al., 2022) and for the global ocean ($12\text{--}185 \text{ ng g}^{-1} \text{ dw}$) (Zhang et
345 al., 2020; Wu et al., 2021).

346 Chouvelon et al. (2019) showed that Hg bioaccumulation in the lowest size-fractions ($6\text{--}60$
347 μm) may be high compared to larger plankton size-fractions. The higher surface-to-volume
348 ratio (giving a higher contact surface), which increases Hg uptake (Fisher, 1985), may explain
349 the higher concentrations of THg measured in picoplankton in our study. Small phytoplankton
350 cells are prevalent in Mediterranean oligotrophic waters and during our sampling survey
351 (Boudriga et al., 2022). Enhanced concentrations of MeHg have previously been observed in
352 sea water during pico- and nanoplankton blooms in the Mediterranean Sea (Heimbürger et al.,
353 2010).

354 Low dissolved Hg (dHg) and MMHg (dMHg) concentrations measured in this study (94 ± 32
355 pg L^{-1} and $13 \pm 7 \text{ pg L}^{-1}$, respectively, Table S6) are likely due to enhanced photochemistry
356 and evasion (Cossa et al., 2009; Sunderland et al., 2009; Heimbürger et al., 2010; Cossa et al.,
357 2022). The mean BCF_{THg} values in the $0.7\text{--}2.7$ and $2.7\text{--}20 \mu\text{m}$ fractions were $2 \times 10^6 \text{ L kg}^{-1}$
358 dw and $1 \times 10^6 \text{ L kg}^{-1} \text{ dw}$, respectively, while the mean BCF_{MMHg} values were $1 \times 10^5 \text{ L kg}^{-1}$
359 dw and $8 \times 10^5 \text{ L kg}^{-1} \text{ dw}$, respectively (Table S7). Mediterranean phytoplankton of different

360 size classes bioconcentrate THg and MMHg 10^6 and 10^5 times, respectively, from sea water,
361 these values being in the upper range of those reported in the literature (Table S5). The mean
362 THg bioconcentration values observed in this study are >10 times higher than the partitioning
363 coefficient of suspended particulate matter (K_d), generally used in global THg models (Zhang
364 et al., 2014), which testifies to the need for more accurate regional data. Various studies have
365 already highlighted the underestimation of K_d , constraining Hg export fluxes from the surface
366 and, more broadly, its biogeochemical cycle (Lamborg et al., 2016; Tesán-Onrubia et al.,
367 2020). It has also been observed that MMHg bioconcentration was promoted under low
368 dissolved organic carbon concentrations (Schartup et al., 2018).

369 The MERITE-HIPPOCAMPE cruise offered a unique opportunity to couple biological and
370 contaminant analyses (Tedetti et al., 2023), and explore for the first time the relationships
371 between the composition of the suspended particles collected, and their THg and MMHg
372 concentrations. Suspended particles collected on filters were a complex mixture of living and
373 dead organisms (autotrophic and heterotrophic), also containing detritus and mineral particles.
374 Tesán-Onrubia et al. (2023) showed that the 0.7–2.7 and 2.7–20 μm size-fractions were
375 dominated (86% of the total biomass) by two phytoplankton groups: *Synechococcus* spp. (~1
376 μm) and nanoeukaryotes (~4 μm). The two axes of the PCA analysis relating THg and
377 MMHg concentrations to the size class and group composition of phytoplankton explained
378 56% of the variability (Fig. S1). Higher THg concentrations were associated with a
379 dominance of *Prochlorococcus* spp. (~0.5 μm) in the 0.7–2.7 μm size-fraction, and a
380 dominance of nanoeukaryotes in the 2.7–20 μm size-fraction. Similarly, higher MMHg
381 concentrations were related to the dominance of *Synechococcus* spp. in the 0.7–2.7 μm size-
382 fraction, and to the dominance of *Cryptophyceae* (~6 μm) in the 2.7–20 μm size-fraction.
383 These two phytoplankton size-fractions constitute a large part of the diet of zooplankton
384 organisms between 200 and 1000 μm size, and represent an important source of Hg for
385 consumers (Tesán-Onrubia et al., 2023).

3.2 THg and MMHg in zooplankton

389 THg and MMHg bioaccumulated with size among zooplankton, their concentrations
390 increasing from 22 to 45 ng g^{-1} dw, and from 3 to 7 ng g^{-1} dw, respectively, in 60 to 2000 μm
391 size-fractions (Fig. 2a, 2b, Tables S3, S4). Bioaccumulation of MMHg with zooplankton size
392 was previously shown in the North Atlantic (Hammerschmidt et al., 2013), while no

393 difference was found for THg in the Mediterranean (Chouvelon et al., 2019). THg and MMHg
394 concentration values reported here in the Mediterranean zooplankton were comparable to
395 those observed in other regions (Table S8) (Stern and Macdonald, 2005; Hammerschmidt and
396 Fitzgerald, 2006; Loseto et al., 2008; Lavoie et al., 2010; Cossa et al., 2012; Hammerschmidt
397 et al., 2013; Gosnell and Mason, 2015; Gosnell et al., 2017; Harding et al., 2018), but were
398 lower than those from the Arctic Ocean (Campbell et al., 2005; Foster et al., 2012; Pućko et
399 al., 2014; Fox et al., 2017) and from one study in the Mediterranean Sea (Buckman et al.,
400 2018). Our measured MMHg concentrations in zooplankton are in relatively good agreement
401 with model outputs for the Mediterranean Sea (3–10 ng g⁻¹ dw) (Rosati et al., 2022) and the
402 global ocean (1–69 ng g⁻¹ dw) (Zhang et al., 2020; Wu et al., 2021).

403 Changes in metabolism during an organism's life cycle may impact its MMHg concentration.
404 Hammerschmidt and Fitzgerald (2006) showed reduced removal and higher uptake rates in
405 large-size organisms compared to smaller ones. Fierro-González et al. (2023) reported an
406 increase in carnivory with increasing size of zooplankton, which was also in agreement with
407 increasing trophic level traced by $\delta^{15}\text{N}$ (Tesán-Onrubia et al., 2023). The lowest THg and the
408 highest MMHg concentrations were both measured in the largest size-fraction (>2000 μm)
409 (Table S3, S4 and S9), as observed in previous studies (Chouvelon et al., 2019).

410 The biochemical composition of zooplankton may also explain the accumulation of THg and
411 particularly MMHg. MMHg concentrations were significantly correlated with particulate
412 organic carbon (POC), proteins and lipids in zooplankton ($R^2 = 0.47$, $p < 0.0001$; $R^2 = 0.18$, p
413 $= 0.009$ and $R^2 = 0.25$, $p = 0.002$, respectively). The quantity of these compounds increased
414 with the size of zooplankton, except for the >2000 μm fraction (Tesan-Onrubia et al., 2023).
415 The affinity of Hg for POC and proteins is due to the capacity of thiol groups present in
416 cellular proteins to effectively bind to Hg and MMHg (Ravichandran, 2004; Yoon et al.,
417 2005; Gosnell and Mason, 2015).

3.3 Trophic transfer of THg and MMHg

420 Trophic transfer in the plankton food web was assessed taking into consideration all phyto-
421 and zooplankton size-fractions. The two smallest size-fractions of phytoplankton (0.7–2.7 and
422 2.7–20 μm) presented the highest THg but the lowest MMHg concentrations with respect to
423 most zooplankton size-fractions ($H = 23.9$, $p < 0.0001$ and $H = 30.1$, $p < 0.0001$, respectively)
424 (Fig. 2a, 2b, Tables S3, S4). While THg concentrations were related mainly to the effect of
425 the surface-volume ratio on bioconcentration in phytoplankton, MMHg concentrations were

426 mainly related to predation relationships and biomagnification processes among zooplankton
427 fractions. Biomagnification was assessed by using the $\delta^{15}\text{N}$ as a proxy of trophic level (Fig.
428 3). The logTHg and logMMHg showed respectively negative and positive correlations with
429 $\delta^{15}\text{N}$ ($R^2 = 0.1$, $p < 0.05$ and $R^2 = 0.43$, $p < 0.0001$, respectively, $n = 57$), indicating a
430 bioreduction of THg ($\text{TMF}_{\text{THg}} = 0.9$) and a biomagnification of MMHg in the food web
431 studied ($\text{TMF}_{\text{MMHg}} = 1.7$). In our work, particularly low TMF_{THg} were recorded, indicating a
432 marked bioreduction of THg within the planktonic food web. Chouvelon et al. (2009) also
433 observed no THg increase in zooplankton fractions of increasing size, and THg
434 biomagnification in the food web only when zooplanktivorous fishes were considered. In our
435 case, when only zooplankton size-fractions $>60 \mu\text{m}$ were considered, significant positive
436 correlations were observed for both logTHg and logMMHg and $\delta^{15}\text{N}$ ($R^2 = 0.22$, $p < 0.005$
437 and $R^2 = 0.39$, $p < 0.0001$, respectively), thus evidencing the biomagnification of THg
438 ($\text{TMF}_{\text{THg}} = 1.3$) and a higher biomagnification factor of MMHg ($\text{TMF}_{\text{MMHg}} = 2.1$).
439 The high proportions of MMHg, exceeding 95% in higher trophic level consumers (UNEP,
440 2019), as well as the lack of data in the literature regarding primary producers and particularly
441 pico- and nanoplankton, may explain these differences. The plankton TMF_{MMHg} in our study
442 showed high values compared to other marine food webs, which also included higher trophic
443 level organisms (Atwell et al., 1998; Campbell et al., 2005; Al-Reasi et al., 2007; Nfon et al.,
444 2009; Lavoie et al., 2010, 2013; Cossa et al., 2012; Chouvelon et al., 2018; Harding et al.,
445 2018; Hilgendorf et al., 2022). Low growth rates, specific to the oligotrophic Mediterranean
446 Sea, seem to induce higher MMHg biomagnification in planktivorous food webs (Cossa et al.,
447 2012; Chouvelon et al., 2018). The %MMHg significantly increased between phyto- and
448 zooplankton groups from a mean of 3% in the $0.7\text{--}20 \mu\text{m}$ fractions to 23% in the $>60 \mu\text{m}$
449 fraction ($H = 35.8$, $p < 0.0001$) (Fig. 2c), highlighting the preferred biomagnification of
450 MMHg. Inorganic Hg has a lower assimilation efficiency compared to MMHg, while their
451 efflux rates are similar (Mason et al., 1996; Lawson and Mason, 1998; Lee and Fisher, 2017),
452 explaining the inverted patterns between food sources and consumers. Inorganic Hg reacts in
453 the same way as other trace metals (Chen and Folt, 2000; Ho et al., 2007; Chouvelon et al.,
454 2019; Chifflet et al., 2023). To our knowledge, there is no previous estimation of MMHg
455 biomagnification in plankton food web considering different size-fractions of phyto- and
456 zooplankton. The few studies that have explored this point consisted of models for the
457 Mediterranean Sea (Rosati et al., 2022) and the global ocean (Zhang et al., 2020; Wu et al.,
458 2021). Without exception, these models indicate bioreduction of MMHg in plankton food

459 webs, mainly composed of herbivorous and omnivorous organisms, and biomagnification
460 when carnivorous organisms were taken into consideration. Our results suggest the contrary,
461 biomagnification of MMHg occurs in all plankton consumers, independently of their trophic
462 position.

463 The trophic transfer efficiency between phytoplankton (0.7–2.7 and 2.7–20 μm) and
464 zooplankton size-fractions ($>60 \mu\text{m}$) was assessed by considering the total amounts of THg
465 and MMHg available in their respective biomasses at the CML (Fig. 4). THg amounts in
466 phyto- and zooplankton biomass was 15 and 1 ng m^{-3} of sea water, respectively, while their
467 respective MMHg contents amounted to 200 and 300 pg m^{-3} . MMHg is almost 10 times
468 higher than that modeled in the Mediterranean Sea (Rosati et al., 2022). The trophic transfer
469 efficiency of THg ranged from 2 to 21% (average 8%), while it was higher for MMHg,
470 ranging from 11 to 169 %, with an average of 78%. Zooplankton can represent a comparable
471 or even larger sink of MMHg when compared to phytoplankton. Longer lifespan together
472 with bioaccumulation can lead to a higher MMHg storage in zooplankton despite their lower
473 biomass than phytoplankton. The MMHg trophic transfer efficiency estimated here presented
474 a higher value than the zooplankton daily grazing, which accounted for 2.7 to 27% of the
475 phytoplankton stock (Fierro-González et al., 2023). Considering daily grazing and Hg
476 concentrations in phytoplankton and assuming a quantitative assimilation of MMHg,
477 zooplankton organisms should have grazed for 6 to 13 days to reach the MMHg
478 concentrations measured in their body. This short integration time suggested that zooplankton
479 could be a good bioindicator of Hg exposure over days or a few weeks. The results reported
480 here indicated that MMHg was efficiently biomagnified and transferred along the plankton
481 food web, in contrast to a rather inefficient transfer of inorganic Hg.

483 3.4 Spatial variability of THg and MMHg

484 Dissolved Hg (dHg) concentrations ranged from 50 to 165 pg L^{-1} at St11 and St4,
485 respectively. Dissolved MeHg (dMeHg) concentrations ranged from detection limits (7 pg L^{-1})
486 at St1, St9, St11, St17 and St19 to 26 pg L^{-1} in St3. Both Hg species were comparable to
487 previous studies in the Mediterranean Sea (Jiskra et al., 2021; Cossa et al., 2022).

488 THg and MMHg concentrations in phytoplankton (0.7–20 μm) showed strong spatial
489 variations in the western Mediterranean, with the highest values in the smallest fraction
490 recorded at St1 (Toulon in the north) and St17 (Gabès in the south) (Table S3 and S4).

491 Volume concentrations of MMHg in the 0.7 to 20 μm fractions (in pg L^{-1}) were significantly

492 correlated to phytoplankton biomass ($R^2 = 0.49$, $p < 0.001$) (Table S10). This highlighted the
493 influence of the biomass on Hg-uptake at the basis of the plankton food web. Zones with high
494 biomass of small phytoplankton cells may store a large amount of Hg in phytoplankton,
495 bioavailable then for grazers and higher trophic level consumers. In addition, inorganic Hg
496 may represent a substrate for MMHg production.

497 Our results suggested higher THg and especially MMHg differences in zooplankton between
498 stations than between size-fractions (Fig. 5, Table S3 and S4). The high growth rates and
499 short life cycles of zooplankton make it a potentially relevant biomonitor for ambient MMHg
500 concentrations over short periods, as suggested in the previous section. This observation
501 contrasts with the high variability reported in marine organisms of higher trophic level related
502 in particular to longer life span and larger home ranges (UNEP, 2019).

503 THg and MMHg concentrations of zooplankton size-fractions available at all stations (60–
504 200, 200–500 and *500–1000 μm , *unavailable for St17) were pooled to test zooplankton
505 spatial variability that appeared higher for MMHg than for THg (Fig. 5). Significant
506 differences were reported between stations only for MMHg ($H = 24.0$, $p = 0.004$). Mean
507 MMHg concentrations differed ten-fold between minimum ($0.6 \text{ ng g}^{-1} \text{ dw}$, St17) and
508 maximum values ($9.4 \text{ ng g}^{-1} \text{ dw}$, St1). This highlighted the importance of measuring MMHg
509 in consumers with lower trophic levels. Zooplankton from northern (St1, 2, 3 and 4) and
510 offshore (St9, 10 and 11) areas presented higher MMHg concentrations than those from the
511 southern area (St15, 17 and 19) ($H = 14.0$, $p = 0.001$). A $\text{TMF}_{\text{MMHg}} < 1$ indicated a
512 bioreduction of MMHg in zooplankton and consequently a lower exposure to Hg of
513 zooplankton along the Tunisian coast (St17 and 19). (Fig. 6).

514 The two axes of the PCA analysis, performed between THg, MMHg, POC, C/N, protein,
515 lipids, $\delta^{13}\text{C}$, $\delta^{15}\text{N}$, and biomass values in zooplankton per station, explained 57% of the
516 variability (Fig. S2). Two groups of stations were observed along the first axis: the first group
517 gathering St1, 2, 9, 10 and 11, and the second one including St3, 4, 15, 17, and 19. The first
518 group was related to high concentrations in POC, proteins, lipids, THg, MMHg, trophic level
519 and $\delta^{15}\text{N}$ in zooplankton, while the second group was correlated with high values of C/N, $\delta^{13}\text{C}$
520 and zooplankton biomass. MMHg in zooplankton increased with the trophic level ($\delta^{15}\text{N}$ may
521 be used as a proxy). Zooplankton MMHg decreased with increasing amounts of organic
522 matter, likely because of the affinity of POC, proteins and lipids for Hg. MMHg
523 concentrations in zooplankton were high in oligotrophic, low productivity areas with low
524 zooplankton biomass, high trophic level and high POC, protein and lipid content. Under

525 oligotrophic conditions, zooplankton were limited by food resources and, as a result, their
1 526 biomass and growth rates decreased, and increasing Hg bioaccumulation was observed.
2
3 527 Oligotrophic ecosystems also have longer food webs with intermediate consumers (ciliates,
4
5 528 dinoflagellates, microzooplankton, etc.), which may constitute a trophic link between pico-
6
7 529 and nanoplankton, and mesozooplankton, generating additional food steps and probably
8
9 530 increasing the biomagnification processes (Søreide et al., 2006; Kürten et al., 2013).
10
11 531 The negative correlation in zooplankton between MMHg and its biomass may suggest a
12
13 532 biodilution with growth in more productive areas. This is probably the case in the Gulf of
14
15 533 Gabès where lower Hg concentrations in planktivorous species were already reported
16
17 534 compared to those in the north-western Mediterranean basin (Aboul-Dahab et al., 1986; Ben
18 535 Hassine et al., 1990; Joiris et al., 1999). Moreover, in ecosystems where nutrients and
19
20 536 phytoplankton resources are abundant, herbivory is the main food pathway, generating lower
21
22 537 trophic level ecosystems (Sommer et al., 2002) and thus potentially lower Hg concentrations
23
24 538 in consumers.
25
26 539 Coastal areas have been considered to be hotspots for Hg-accumulation due to proximity to
27 540 sediment and resuspension (Chen et al., 2008). Cossa et al. (2018) showed that MeHg
28
29 541 concentrations in subsurface waters are higher in Mediterranean offshore waters. Although
30
31 542 coastal regions are subjected to additional sources of Hg (submarine groundwater discharge,
32
33 543 rivers and sediments), our results evidenced a lower trophic transfer of Hg in plankton food
34
35 544 webs compared to offshore areas, as also observed by Cossa et al. (2012) in the Gulf of Lion.
36
37 545 There is indeed more and more evidence of *in situ* Hg methylation in oxygenated waters of
38 546 the open ocean (Mason and Fitzgerald, 1990; Blum et al., 2013; Masbou et al., 2015; Villar et
39
40 547 al. 2020; Liu et al., 2021), and the Mediterranean Sea (Cossa et al. 2022).
41
42 548 However, potential sources of Hg in contaminated areas must be considered as well. Toulon
43
44 549 Bay represents an important hotspot of Hg, containing large amounts in its sediments (Tessier
45
46 550 et al., 2011) and may be responsible for the highest concentrations measured in this study.
47
48 551 High concentrations of THg and MMHg have already been recorded in fish and mussels in
49 552 Toulon Bay (Cresson et al., 2014; Briant et al., 2017).
50

51 553

52 554 **4. Conclusions**

53 555

54
55
56 556 Few Hg data are currently available for plankton, particularly for MMHg, and they generally
57
58 557 show wide variations. An inappropriate plankton sampling strategy may lead to the collection
59

60

61

62

63

64

65

558 of organisms with a heterogenous size and composition, highly impacting their Hg and
1 559 MMHg concentrations. We have tried to overcome these limitations with a dedicated
2
3 560 sampling strategy for the acquisition of different phyto- and zooplankton size-classes, the
4
5 561 acquisition of trophic proxies and the collection of sufficient biomass for complementary
6
7 562 biological and chemical analyses.

8
9 563 High THg and MMHg bioconcentration values were observed for phytoplankton, with the
10
11 564 highest values for picoplankton. Small phytoplankton cells were the main contributors to
12
13 565 primary production in the Mediterranean waters during our sampling campaign and a major
14
15 566 food source for zooplankton. Phytoplankton THg concentrations were higher overall
16
17 567 compared to the existing literature. Our study implies that phytoplankton in the oligotrophic
18 568 Mediterranean Sea is an important driver in the biomagnification of MMHg.

19
20 569 Although THg accumulation through diet is a widely accepted process, our results show that
21
22 570 THg bioreduces while MMHg bioaccumulates in the plankton food web. Different kinetics of
23
24 571 iHg and MMHg have been evidenced in plankton, supporting the need to analyze both phyto-
25
26 572 and zooplankton, and to relate them to their species/group composition in future studies.

27 573 Biomagnification of MMHg in all plankton consumers was evidenced, independently of their
28
29 574 trophic position. High biomagnification factors were measured compared to previous studies,
30
31 575 suggesting an effective transfer in Mediterranean plankton food webs.

32
33 576 Moreover, the biochemical composition of zooplankton, particularly the availability of POC,
34
35 577 proteins and lipids appears to have an important role in MMHg bioaccumulation.

36 578 Spatial variability in MMHg concentrations in zooplankton was important, with ten-fold
37
38 579 differences between areas. Productivity gradients may explain these contrasts. Higher
39
40 580 zooplankton MMHg concentrations were measured in low productive areas offshore. In
41
42 581 contrast, more productive coastal planktonic food webs showed lower zooplankton MMHg
43
44 582 concentrations. Our results suggest a lower impact of Hg on plankton food webs in the less
45
46 583 poorly-studied southern Mediterranean Sea, but more observations are needed to corroborate
47
48 584 this. Oligotrophy and plankton trophodynamics were key factors in the transfer of Hg in the
49
50 585 Mediterranean Sea, playing probably an important role in the Hg transfer along food webs.
51
52 586 Our study may thus contribute to explaining the higher Hg levels observed in Mediterranean
53
54 587 apex predators. The impact of climate change is thought to contribute to the increase of the
55
56 588 oligotrophy and the decrease in size of phytoplankton and may thus exacerbate Hg
57
58 589 accumulation in Mediterranean marine food webs in the future. Overall, our study suggests
59
60 590 that bioconcentration of MMHg into phytoplankton and subsequent bioaccumulation and

591 biomagnification are by far the most important factors driving higher trophic level MMHg
1
2 592 exposure. As such, the efforts in reducing Hg emissions within the Minamata Convention may
3
4 593 be outweighed by the effects of climate change on the lower marine food web structure.

5 594
6
7
8
9
10
11
12
13
14
15
16
17
18
19
20
21
22
23
24
25
26
27
28
29
30
31
32
33
34
35
36
37
38
39
40
41
42
43
44
45
46
47
48
49
50
51
52
53
54
55
56
57
58
59
60
61
62
63
64
65

595 **Author contribution statement**

1
2 596 Conception and design of study: DB, LEHB, FC, MT, JK

3
4 597 Acquisition of data: JATO, JK, BT, MT, FC

5
6 598 Analysis and/or interpretation of data: JATO, DB, LEHB, MHV, MT, AD, BT, JK

7
8 599 Drafting of the manuscript: JATO, DB, LEHB, MHV, MT

9
10 600 Revising/editing of the manuscript: JATO, DB, LEHB, MHV, AD, MVL, IGA, JK, BT, FC,

11 601 MT

12
13 602 Project administration and funding acquisition: DB, MT, FC

14
15 603

16 604 **Acknowledgements**

17
18 605 The authors wish to thank the crew of the R/V Antea and the various platforms of the

19
20 606 Mediterranean Institute of Oceanography which have contributed to the data acquisition:

21
22 607 Plateforme Analytique de Chimie des Environnements Marins (PACEM) for the POC/PON

23
24 608 measurements, Plateforme Régionale de Cytométrie pour la Microbiologie (PRECYM) for

25
26 609 cytometric analyses, Microscopie et Imagerie numérique (MIM) for identification expertise

27
28 610 and the Service Atmosphère-Mer (SAM) for the technical and operational tasks. The authors

29
30 611 thank the LIENSs joint research unit (CNRS - La Rochelle University) for the measurement

31
32 612 of $\delta^{13}\text{C}$ and $\delta^{15}\text{N}$ values. The MERITE-HIPPOCAMPE project has been funded by the cross-

33
34 613 disciplinary Pollution & Contaminants axis of the CNRS-INSU MISTRALS program (joint

35
36 614 action of the MERMEX-MERITE and CHARMEX subprograms) and received support from

37
38 615 the IRD French-Tunisian International Joint Laboratory (LMI) COSYS-Med. We are grateful

39
40 616 for the additional funding received from IFREMER, the MIO Action Sud and Transverse

41
42 617 Axis programs (CONTAM Transversal Axis), and from the IRD Ocean Department. This

43
44 618 study received funding by the CONTAMPUMP project (ANR JCJC #19-CE34-0001-01). We

45
46 619 warmly thank Michael Paul for improvement of the English. Finally, we acknowledge two

47
48 620 reviewers for their helpful and constructive comments and suggestions.

49
50 621

51 622 **Supplementary information**

52
53 623 Supplementary material related to this article is available online.

54

55

56

57

58

59

60

61

62

63

64

65

624 **References**

- 1
2 625 Aboul-Dahab, O., Halim, Y. and ElRayis, O.,1986. Mercury species in coastal marine organisms
3 626 from different trophic levels west of Alexandria. In FAO/UNEP/WHO/IOC/IAEA
4 627 Meeting on the biogeochemical cycle of mercury in the Mediterranean. FAO Fish
5 628 Report. No. 325 (suppl), Rome, pp. 1-7.
6
7 629 Al-Reasi, H.A., Ababneh, F.A., Lean, D.R., 2007. Evaluating mercury biomagnification in fish
8 630 from a tropical marine environment using stable isotopes ($\delta^{13}C$ and $\delta^{15}N$).
9 631 Environmental Toxicology and Chemistry 26, 1572–1581. [https://doi.org/10.1897/06-](https://doi.org/10.1897/06-359R.1)
10 632 359R.1
11 633 Aston, S.R., Fowler, S.W., 1985. Mercury in the open Mediterranean: evidence of
12 634 contamination? Science of the Total Environment 43, 13–26.
13 635 [https://doi.org/10.1016/0048-9697\(85\)90028-2](https://doi.org/10.1016/0048-9697(85)90028-2)
14
15 636 Atwell, L., Hobson, K.A., Welch, H.E., 1998. Biomagnification and bioaccumulation of mercury
16 637 in an arctic marine food web: insights from stable nitrogen isotope analysis. Canadian
17 638 Journal of Fisheries and Aquatic Sciences. 55, 1114–1121. [https://doi.org/10.1139/f98-](https://doi.org/10.1139/f98-001)
18 639 001
19
20 640 Bacci, E., 1989. Mercury in the Mediterranean. Marine Pollution Bulletin 20, 59–63.
21 641 [https://doi.org/10.1016/0025-326X\(89\)90227-0](https://doi.org/10.1016/0025-326X(89)90227-0)
22
23 642 Baeyens, W., Leermakers, M., Papina, T., Saprykin, A., Brion, N., Noyen, J., De Gieter, M.,
24 643 Elskens, M., Goeyens, L., 2003. Bioconcentration and biomagnification of mercury and
25 644 methylmercury in North Sea and Scheldt estuary fish. Archives of Environmental
26 645 Contamination and Toxicology 45, 498–508. [https://doi.org/10.1007/s00244-003-2136-](https://doi.org/10.1007/s00244-003-2136-4)
27 646 4
28
29 647 Bănar, D., Diaz, F., Verley, P., Campbell, R., Navarro, J., Yohia, C., Oliveros-Ramos, R.,
30 648 Mellon-Duval, C., Shin, Y.-J., 2019. Implementation of an end-to-end model of the Gulf
31 649 of Lions ecosystem (NW Mediterranean Sea). I. Parameterization, calibration and
32 650 evaluation. Ecological Modelling 401, 1–19.
33 651 <https://doi.org/10.1016/j.ecolmodel.2019.03.005>
34
35 652 Bănar, D., Mellon-Duval, C., Roos, D., Bigot, J.-L., Souplet, A., Jadaud, A., Beaubrun, P.,
36 653 Fromentin, J.-M., 2013. Trophic structure in the Gulf of Lions marine ecosystem (north-
37 654 western Mediterranean Sea) and fishing impacts. Journal of Marine Systems 111–112,
38 655 45–68. <https://doi.org/10.1016/j.jmarsys.2012.09.010>
39
40 656 Bargagli, R., Monaci, F., Sanchez-Hernandez, J.C., Cateni, D., 1998. Biomagnification of

- 657 mercury in an Antarctic marine coastal food web. *Marine Ecology Progress Series* 169,
1 658 65–76. <https://doi.org/10.3354/meps169065>
- 3 659 Bełdowska, M., Kobos, J., 2018. The variability of Hg concentration and composition of marine
4 660 phytoplankton. *Environmental Science Pollution Research* 25, 30366–30374.
5 661 <https://doi.org/10.1007/s11356-018-2948-4>
- 7 662 Ben-Hassine, O. K., Raibaut, A., Ben Souissi, J. and Rousset, L., 1990. Morphologie de
8 663 *Peroderma cylindricum* (Heller, 1865), Copépode parasite de la *Sardina pilchardus*
9 664 (Walbaum, 1792) et quelques aspects de son écologie dans les eaux côtières tunisiennes.
10 665 *Annales des Sciences naturelles, Zoologie Paris* 13(11), 9-16.
- 12 666 Bishop, J.K.B., Lam, P.J., Wood, T.J., 2012. Getting good particles: Accurate sampling of
13 667 particles by large volume in-situ filtration: Getting good particles. *Limnology and*
14 668 *Oceanography: Methods* 10, 681–710. <https://doi.org/10.4319/lom.2012.10.681>
- 16 669 Blum, J.D., Popp, B.N., Drazen, J.C., Anela Choy, C., Johnson, M.W., 2013. Methylmercury
17 670 production below the mixed layer in the North Pacific Ocean. *Nature Geosciences* 6,
18 671 879–884. <https://doi.org/10.1038/ngeo1918>
- 20 672 Boudriga, I., Thyssen, M., Zouari, A., Garcia, N., Tedetti, M., Bel Hassen, M., 2022.
21 673 Ultraphytoplankton community structure in subsurface waters along a North-South
22 674 Mediterranean transect. *Marine Pollution Bulletin* 182, 113977.
23 675 <https://doi.org/10.1016/j.marpolbul.2022.113977>
- 25 676 Briant, N., Chouvelon, T., Martinez, L., Brach-Papa, C., Chiffolleau, J., Savoye, N., Sonke, J.,
26 677 Knoery, J., 2017. Spatial and temporal distribution of mercury and methylmercury in
27 678 bivalves from the French coastline. *Marine Pollution Bulletin* 114, 1096–1102.
28 679 <https://doi.org/10.1016/j.marpolbul.2016.10.018>
- 30 680 Buckman, K.L., Lane, O., Kotnik, J., Bratkic, A., Sprovieri, F., Horvat, M., Pirrone, N., Evers,
31 681 D.C., Chen, C.Y., 2018. Spatial and taxonomic variation of mercury concentration in
32 682 low trophic level fauna from the Mediterranean Sea. *Ecotoxicology* 27, 1341–1352.
33 683 <https://doi.org/10.1007/s10646-018-1986-5>
- 35 684 Campbell, L.M., Norstrom, R.J., Hobson, K.A., Muir, D.C.G., Backus, S., Fisk, A.T., 2005.
36 685 Mercury and other trace elements in a pelagic Arctic marine food web (Northwater
37 686 Polynya, Baffin Bay). *Science of The Total Environment* 351–352, 247–263.
38 687 <https://doi.org/10.1016/j.scitotenv.2005.02.043>
- 40 688 Carlotti, F., Thibault-Botha, D., Nowaczyk, A., Lefèvre, D., 2008. Zooplankton community
41 689 structure, biomass and role in carbon fluxes during the second half of a phytoplankton

- 690 bloom in the eastern sector of the Kerguelen Shelf (January–February 2005). *Deep Sea*
1 691 *Research Part II: Topical Studies in Oceanography* 55, 720–733.
2
3 692 <https://doi.org/10.1016/j.dsr2.2007.12.010>
4
- 5 693 Charette, T., Rosabal, M., Amyot, M., 2021. Mapping metal (Hg, As, Se), lipid and protein
6 694 levels within fish muscular system in two fish species (Striped Bass and Northern Pike).
7
8 695 *Chemosphere* 265, 129036. <https://doi.org/10.1016/j.chemosphere.2020.129036>
9
- 10 696 Chen, C.Y., Folt, C.L., 2000. Bioaccumulation and Diminution of Arsenic and Lead in a
11 697 Freshwater Food Web. *Environmental Science & Technology* 34, 3878–3884.
12
13 698 <https://doi.org/10.1021/es991070c>
14
15
- 16 699 Chen, C., Amirbahman, A., Fisher, N., Harding, G., Lamborg, C., Nacci, D., Taylor, D., 2008.
17 700 Methylmercury in Marine Ecosystems: Spatial Patterns and Processes of Production,
18
19 701 Bioaccumulation, and Biomagnification. *EcoHealth* 5, 399–408.
20
21 702 <https://doi.org/10.1007/s10393-008-0201-1>
22
- 23 703 Chifflet, S., Briant, N., Tesán-Onrubia, J.A., Zaaboub, N., Amri, S., Radakovitch, O., Bănaru,
24 704 D., Tedetti, M., 2023. Distribution and accumulation of trace metal in the planktonic
25
26 705 food web of the Mediterranean Sea (MERITE-HIPPOCAMPE campaign). *Marine*
27
28 706 *Pollution Bulletin* 186, 114384. <https://doi.org/10.1016/j.marpolbul.2022.114384>.
29
- 30 707 Chouvelon, T., Cresson, P., Bouchouca, M., Brach-Papa, C., Bustamante, P., Crochet, S.,
31
32 708 Marco-Miralles, F., Thomas, B., Knoery, J., 2018. Oligotrophy as a major driver of
33
34 709 mercury bioaccumulation in medium-to high-trophic level consumers: A marine
35
36 710 ecosystem-comparative study. *Environmental Pollution* 233, 844–854.
37
38 711 <https://doi.org/10.1016/j.envpol.2017.11.015>
39
- 40 712 Chouvelon, T., Strady, E., Harmelin-Vivien, M., Radakovitch, O., Brach-Papa, C., Crochet, S.,
41
42 713 Knoery, J., Rozuel, E., Thomas, B., Tronczynski, J., Chiffolleau, J.-F., 2019. Patterns of
43
44 714 trace metal bioaccumulation and trophic transfer in a phytoplankton-zooplankton-small
45
46 715 pelagic fish marine food web. *Marine Pollution Bulletin* 146, 1013–1030.
47
48 716 <https://doi.org/10.1016/j.marpolbul.2019.07.047>
49
- 50 717 Cinnirella, S., Bruno, D.E., Pirrone, N., Horvat, M., Živković, I., Evers, D.C., Johnson, S.,
51
52 718 Sunderland, E.M., 2019. Mercury concentrations in biota in the Mediterranean Sea, a
53
54 719 compilation of 40 years of surveys. *Scientific Data* 6, 205.
55
56 720 <https://doi.org/10.1038/s41597-019-0219-y>
57
- 58 721 Cossa, D., Martin, J.-M., 1991. Mercury in the Rhône delta and adjacent marine areas. *Marine*
59
60 722 *Chemistry, Reactivity of Chemical Species in Aquatic Environments* 36, 291–302.
61
62
63
64
65

- 723 [https://doi.org/10.1016/S0304-4203\(09\)90067-6](https://doi.org/10.1016/S0304-4203(09)90067-6)
- 1
2 724 Cossa, D., Coquery, M., 2005. The Mediterranean Mercury Anomaly, a Geochemical or a
3
4 725 Biological Issue, in: Saliot, A. (Ed.), The Mediterranean Sea. Springer Berlin
5
6 726 Heidelberg, Berlin, Heidelberg, pp. 177–208. <https://doi.org/10.1007/b107147>
- 7 727 Cossa, D., Averty, B., Pirrone, N., 2009. The origin of methylmercury in open Mediterranean
8
9 728 waters. *Limnology and Oceanography* 54, 837–844.
10
11 729 <https://doi.org/10.4319/lo.2009.54.3.0837>
- 12
13 730 Cossa, D., Harmelin-Vivien, M., Mellon-Duval, C., Loizeau, V., Averty, B., Crochet, S., Chou,
14
15 731 L., Cadiou, J.-F., 2012. Influences of Bioavailability, Trophic Position, and Growth on
16
17 732 Methylmercury in Hakes (*Merluccius merluccius*) from Northwestern Mediterranean
18
19 733 and Northeastern Atlantic. *Environmental Science & Technology* 46, 4885–4893.
20
21 734 <https://doi.org/10.1021/es204269w>
- 22 735 Cossa, D., Knoery, J., Bănaru, D., Harmelin-Vivien, M., Sonke, J.E., Hedgecock, I.M., Bravo,
23
24 736 A.G., Rosati, G., Canu, D., Horvat, M., Sprovieri, F., Pirrone, N., Heimbürger-Boavida,
25
26 737 L.-E., 2022. Mediterranean Mercury Assessment 2022: An Updated Budget, Health
27
28 738 Consequences, and Research Perspectives. *Environmental Science & Technology* 56,
29
30 739 3840–3862. <https://doi.org/10.1021/acs.est.1c03044>
- 31 740 Covelli, S., Faganeli, J., Horvat, M., Brambati, A., 2001. Mercury contamination of coastal
32
33 741 sediments as the result of long-term cinnabar mining activity (Gulf of Trieste, northern
34
35 742 Adriatic sea). *Applied Geochemistry* 16, 541–558.
- 36 743 Cresson, P., Bouchouca, M., Miralles, F., Elleboode, R., Mahé, K., Maruszczak, N., Thebault,
37
38 744 H., Cossa, D., 2015. Are red mullet efficient as bio-indicators of mercury
39
40 745 contamination? A case study from the French Mediterranean. *Marine Pollution Bulletin*
41
42 746 91, 191–199. <https://doi.org/10.1016/j.marpolbul.2014.12.005>
- 43
44 747 Cresson, P., Fabri, M.C., Bouchouca, M., Brach Papa, C., Chavanon, F., Jadaud, A., Knoery, J.,
45
46 748 Miralles, F., Cossa, D., 2014. Mercury in organisms from the Northwestern
47
48 749 Mediterranean slope: Importance of food sources. *Science of The Total Environment*
49
50 750 497–498, 229–238. <https://doi.org/10.1016/j.scitotenv.2014.07.069>
- 51 751 Décima, M., 2022. Zooplankton trophic structure and ecosystem productivity. *Marine Ecology*
52
53 752 *Progress Series* 692, 23–42. <https://doi.org/10.3354/meps14077>
- 54
55 753 Di Benedetto, A.P.M., Bittar, V.T., Camargo, P.B., Rezende, C.E., Kehrig, H.A., 2012. Mercury
56
57 754 and Nitrogen Isotope in a Marine Species from a Tropical Coastal Food Web. *Archives*
58
59 755 *of Environmental Contamination and Toxicology* 62, 264–271.

- 756 <https://doi.org/10.1007/s00244-011-9701-z>
- 1
2 757 Durrieu de Madron, X., Guieu, C., Sempéré, R., Conan, P., Cossa, D., D’Ortenzio, F., Estournel,
3
4 758 C., Gazeau, F., Rabouille, C., Stemmann, L., Bonnet, S., Diaz, F., Koubbi, P.,
5
6 759 Radakovitch, O., Babin, M., Baklouti, M., Bancon-Montigny, C., Belviso, S.,
7
8 760 Bensoussan, N., Bonsang, B., Bouloubassi, I., Brunet, C., Cadiou, J.-F., Carlotti, F.,
9
10 761 Chami, M., Charmasson, S., Charrière, B., Dachs, J., Doxaran, D., Dutay, J.-C., Elbaz-
11
12 762 Poulichet, F., Eléaume, M., Eyrolles, F., Fernandez, C., Fowler, S., Francour, P.,
13
14 763 Gaertner, J.C., Galzin, R., Gasparini, S., Ghiglione, J.-F., Gonzalez, J.-L., Goyet, C.,
15
16 764 Guidi, L., Guizien, K., Heimbürger, L.-E., Jacquet, S.H.M., Jeffrey, W.H., Joux, F., Le
17
18 765 Hir, P., Leblanc, K., Lefèvre, D., Lejeusne, C., Lemé, R., Loÿe-Pilot, M.-D., Mallet, M.,
19
20 766 Méjanelle, L., Mélin, F., Mellon, C., Mériçot, B., Merle, P.-L., Migon, C., Miller, W.L.,
21
22 767 Mortier, L., Mostajir, B., Mousseau, L., Moutin, T., Para, J., Pérez, T., Petrenko, A.,
23
24 768 Poggiale, J.-C., Prieur, L., Pujo-Pay, M., Pulido-Villena, Raimbault, P., Rees, A.P.,
25
26 769 Ridame, C., Rontani, J.-F., Ruiz Pino, D., Sicre, M.A., Taillandier, V., Tamburini, C.,
27
28 770 Tanaka, T., Taupier-Letage, I., Tedetti, M., Testor, P., Thébault, H., Thouvenin, B.,
29
30 771 Touratier, F., Tronczynski, J., Ulses, C., Van Wambeke, F., Vantrepotte, V., Vaz, S.,
31
32 772 Verney, R., 2011. Marine ecosystems’ responses to climatic and anthropogenic forcings
33 773 in the Mediterranean. *Progress in Oceanography* 91, 97–166.
34
35 774 <https://doi.org/10.1016/j.pocan.2011.02.003>
36
37 775 Fierro-González, P., Pagano, M., Guilloux, L., Makhlof, N., Tedetti, M., Carlotti, F., 2023.
38 776 Zooplankton biomass, size structure, and associated metabolic fluxes with focus on its
39 777 roles at the chlorophyll maximum layer during the plankton-contaminant MERITE-
40 778 HIPPOCAMPE cruise. *Marine Pollution Bulletin* 193, 115056.
41
42 779 <https://doi.org/10.1016/j.marpolbul.2023.115056>
43
44 780 Fisher, N.S., 1985. Accumulation of metals by marine picoplankton. *Marine Biology* 87, 137–
45 781 142. <https://doi.org/10.1007/BF00539421>
46
47 782 Foster, K.L., Stern, G.A., Pazerniuk, M.A., Hickie, B., Walkusz, W., Wang, F., Macdonald,
48 783 R.W., 2012. Mercury Biomagnification in Marine Zooplankton Food Webs in Hudson
49 784 Bay. *Environmental Science & Technology* 46, 12952–12959.
50
51 785 <https://doi.org/10.1021/es303434p>
52
53 786 Fox, A.L., Trefry, J.H., Trocine, R.P., Dunton, K.H., Lasorsa, B.K., Konar, B., Ashjian, C.J.,
54 787 Cooper, L.W., 2017. Mercury biomagnification in food webs of the northeastern
55 788 Chukchi Sea, Alaskan Arctic. *Deep Sea Research Part II: Topical Studies in*

- 789 Oceanography, 144, 63–77. <https://doi.org/10.1016/j.dsr2.2017.04.020>
- 1
2 790 Gosnell, K.J., Balcom, P.H., Tobias, C.R., Gilhooly III, W.P., Mason, R.P., 2017. Spatial and
3
4 791 temporal trophic transfer dynamics of mercury and methylmercury into zooplankton and
5
6 792 phytoplankton of Long Island Sound. *Limnology and Oceanography* 62, 1122–1138.
7
8 793 <https://doi.org/10.1002/lno.10490>
- 9 794 Gosnell, K.J., Mason, R.P., 2015. Mercury and methylmercury incidence and bioaccumulation in
10
11 795 plankton from the central Pacific Ocean. *Marine Chemistry* 177, 772–780.
12
13 796 <https://doi.org/10.1016/j.marchem.2015.07.005>
- 14 797 Guidi, L., Stemmann, L., Jackson, G.A., Ibanez, F., Claustre, H., Legendre, L., Picheral, M.,
15
16 798 Gorskya, G., 2009. Effects of phytoplankton community on production, size, and export
17
18 799 of large aggregates: A world-ocean analysis. *Limnology and Oceanography* 54, 1951–
19
20 800 1963. <https://doi.org/10.4319/lo.2009.54.6.1951>
- 21
22 801 Hammerschmidt, C.R., Finiguerra, M.B., Weller, R.L., Fitzgerald, W.F., 2013. Methylmercury
23
24 802 Accumulation in Plankton on the Continental Margin of the Northwest Atlantic Ocean.
25
26 803 *Environmental Science & Technology* 47, 3671–3677.
27
28 804 <https://doi.org/10.1021/es3048619>
- 29 805 Hammerschmidt, C.R., Fitzgerald, W.F., 2006. Bioaccumulation and Trophic Transfer of
30
31 806 Methylmercury in Long Island Sound. *Archives of Environmental Contamination and*
32
33 807 *Toxicology* 51, 416–424. <https://doi.org/10.1007/s00244-005-0265-7>
- 34
35 808 Harding, G., Dalziel, J., Vass, P., 2018. Bioaccumulation of methylmercury within the marine
36
37 809 food web of the outer Bay of Fundy, Gulf of Maine. *PLOS ONE* 13, e0197220.
38
39 810 <https://doi.org/10.1371/journal.pone.0197220>
- 40 811 Harmelin-Vivien, M., Cossa, D., Crochet, S., Bănar, D., Letourneur, Y., Mellon-Duval, C.,
41
42 812 2009. Difference of mercury bioaccumulation in red mullets from the north-western
43
44 813 Mediterranean and Black seas. *Marine Pollution Bulletin* 58, 679–685.
45
46 814 <https://doi.org/10.1016/j.marpolbul.2009.01.004>
- 47 815 Heimbürger, L.-E., Cossa, D., Marty, J.-C., Migon, C., Averty, B., Dufour, A., Ras, J., 2010.
48
49 816 Methyl mercury distributions in relation to the presence of nano- and picophytoplankton
50
51 817 in an oceanic water column (Ligurian Sea, North-western Mediterranean). *Geochimica*
52
53 818 *et Cosmochimica Acta* 74, 5549–5559. <https://doi.org/10.1016/j.gca.2010.06.036>
- 54
55 819 Heimbürger, L.-E., Sonke, J.E., Cossa, D., Point, D., Lagane, C., Laffont, L., Galfond, B.T.,
56
57 820 Nicolaus, M., Rabe, B., van der Loeff, M.R., 2015. Shallow methylmercury production
58
59 821 in the marginal sea ice zone of the central Arctic Ocean. *Scientific Reports* 5.

- 822 <https://doi.org/10.1038/srep10318>
- 1
2 823 Hilgendag, I.R., Swanson, H.K., Lewis, C.W., Ehrman, A.D., Power, M., 2022. Mercury
3 824 biomagnification in benthic, pelagic, and benthopelagic food webs in an Arctic marine
4
5 825 ecosystem. *Science of The Total Environment* 841, 156424.
6
7 826 <https://doi.org/10.1016/j.scitotenv.2022.156424>
- 8
9 827 Ho, T.-Y., Wen, L.-S., You, C.-F., Lee, D.-C., 2007. The trace metal composition of size-
10
11 828 fractionated plankton in the South China Sea: Biotic versus abiotic sources. *Limnology*
12
13 829 and *Oceanography* 52, 1776–1788. <https://doi.org/10.4319/lo.2007.52.5.1776>
- 14
15 830 Horvat, M., Covelli, S., Faganeli, J., Logar, M., Mandić, V., Rajar, R., Širca, A., Žagar, D., 1999.
16
17 831 Mercury in contaminated coastal environments; a case study: the Gulf of Trieste.
18
19 832 *Science of the Total Environment* 237, 43–56.
- 20
21 833 Hunt, B.P.V., Carlotti, F., Donoso, K., Pagano, M., D’Ortenzio, F., Taillandier, V., Conan, P.,
22
23 834 2017. Trophic pathways of phytoplankton size classes through the zooplankton food
24
25 835 web over the spring transition period in the north-west Mediterranean Sea. *Journal of*
26
27 836 *Geophysical Research: Oceans* 122, 6309–6324. <https://doi.org/10.1002/2016JC012658>
- 28
29 837 Jiskra, M., Heimbürger-Boavida, L.-E., Desgranges, M.-M., Petrova, M.V., Dufour, A., Ferreira-
30
31 838 Araujo, B., Masbou, J., Chmeleff, J., Thyssen, M., Point, D., Sonke, J.E., 2021.
32
33 839 Mercury stable isotopes constrain atmospheric sources to the ocean. *Nature* 597, 678–
34
35 840 682. <https://doi.org/10.1038/s41586-021-03859-8>
- 36
37 841 Joiris, C.R., Holsbeek, L., Laroussi moatemri, N., 1999. Total and Methylmercury in Sardines
38
39 842 *Sardinella aurita* and *Sardina pilchardus* from Tunisia. *Marine Pollution Bulletin* 38,
40
41 843 188–192. [https://doi.org/10.1016/S0025-326X\(98\)00171-4](https://doi.org/10.1016/S0025-326X(98)00171-4)
- 42
43 844 Kehrig, H.A., Palermo, E.F.A., Seixas, T.G., Branco, C.W.C., Moreira, I., Malm, O., 2009.
44
45 845 Trophic transfer of methylmercury and trace elements by tropical estuarine seston and
46
47 846 plankton. *Estuarine, Coastal and Shelf Science* 85, 36–44.
48
49 847 <https://doi.org/10.1016/j.ecss.2009.05.027>
- 50
51 848 Kucuksezgin, F., Altay, O., Uluturhan, E., Kontas, A., 2001. Trace Metal and Organochlorine
52
53 849 Residue Levels in Red Mullet (*Mullus barbatus*) from the Eastern Aegean, Turkey.
54
55 850 *Water Research* 35, 2327–2332. [https://doi.org/10.1016/S0043-1354\(00\)00504-2](https://doi.org/10.1016/S0043-1354(00)00504-2)
- 56
57 851 Kürten, B., Painting, S.J., Struck, U., Polunin, N.V.C., Middelburg, J.J., 2013. Tracking seasonal
58
59 852 changes in North Sea zooplankton trophic dynamics using stable isotopes.
60
61 853 *Biogeochemistry* 113, 167–187. <https://doi.org/10.1007/s10533-011-9630-y>
- 62
63 854 Lamborg, C.H., Hammerschmidt, C.R., Bowman, K.L., Swarr, G.J., Munson, K.M., Ohnemus,
64
65

855 D.C., Lam, P.J., Heimbürger, L.-E., Rijkenberg, M.J.A., Saito, M.A., 2014. A global
1 856 ocean inventory of anthropogenic mercury based on water column measurements.
2
3 857 Nature 512, 65–68. <https://doi.org/10.1038/nature13563>
4
5 858 Lamborg, C.H., Hammerschmidt, C.R., Bowman, K.L., 2016. An examination of the role of
6
7 859 particles in oceanic mercury cycling. *Philosophical Transactions of the Royal Society A*
8
9 860 374, 20150297. <https://doi.org/10.1098/rsta.2015.0297>
10
11 861 Lavoie, R.A., Hebert, C.E., Rail, J.-F., Braune, B.M., Yumvihoze, E., Hill, L.G., Lean, D.R.S.,
12
13 862 2010. Trophic structure and mercury distribution in a Gulf of St. Lawrence (Canada)
14
15 863 food web using stable isotope analysis. *Science of The Total Environment* 408, 5529–
16
17 864 5539. <https://doi.org/10.1016/j.scitotenv.2010.07.053>
18
19 865 Lavoie, R.A., Jardine, T.D., Chumchal, M.M., Kidd, K.A., Campbell, L.M., 2013.
20
21 866 Biomagnification of Mercury in Aquatic Food Webs: A Worldwide Meta-Analysis.
22
23 867 *Environmental Science & Technology*. 47, 13385–13394.
24
25 868 <https://doi.org/10.1021/es403103t>
26
27 869 Lawson, N.M., Mason, R.P., 1998. Accumulation of mercury in estuarine food chains.
28
29 870 *Biogeochemistry* 40, 235–247. <https://doi.org/10.1023/A:1005959211768>
30
31 871 Leblanc, K., Quéguiner, B., Diaz, F., Cornet, V., Michel-Rodriguez, M., Durrieu de Madron, X.,
32
33 872 Bowler, C., Malviya, S., Thyssen, M., Grégori, G., Rembauville, M., Grosso, O.,
34
35 873 Poulain, J., de Vargas, C., Pujo-Pay, M., Conan, P., 2018. Nanoplanktonic diatoms are
36
37 874 globally overlooked but play a role in spring blooms and carbon export. *Nature*
38
39 875 *Communications* 9, 953. <https://doi.org/10.1038/s41467-018-03376-9>
40
41 876 Lee, C.-S., Fisher, N.S., 2016. Methylmercury uptake by diverse marine phytoplankton.
42
43 877 *Limnology and Oceanography* 61, 1626–1639. <https://doi.org/10.1002/lno.10318>
44
45 878 Lee, C.-S., Fisher, N.S., 2017. Bioaccumulation of methylmercury in a marine copepod.
46
47 879 *Environmental Toxicology and Chemistry* 36, 1287–1293.
48
49 880 <https://doi.org/10.1002/etc.3660>
50
51 881 Liu, M., Zhang, Q., Maavara, T., Liu, S., Wang, X., Raymond, P.A., 2021. Rivers as the largest
52
53 882 source of mercury to coastal oceans worldwide. *Nature Geosciences*. 14, 672–677.
54
55 883 <https://doi.org/10.1038/s41561-021-00793-2>
56
57 884 Loseto, L.L., Stern, G.A., Deibel, D., Connelly, T.L., Prokopowicz, A., Lean, D.R.S., Fortier, L.,
58
59 885 Ferguson, S.H., 2008. Linking mercury exposure to habitat and feeding behaviour in
60
61 886 Beaufort Sea beluga whales. *Journal of Marine Systems*, 74, 1012–1024.
62
63 887 <https://doi.org/10.1016/j.jmarsys.2007.10.004>
64
65

- 888 Luengen, A.C., Russell Flegal, A., 2009. Role of phytoplankton in mercury cycling in the San
1 889 Francisco Bay estuary. *Limnology and Oceanography* 54, 23–40.
2
3 890 <https://doi.org/10.4319/lo.2009.54.1.0023>
4
- 5 891 Masbou, J., Point, D., Guillou, G., Sonke, J.E., Lebreton, B., Richard, P., 2015. Carbon Stable
6
7 892 Isotope Analysis of Methylmercury Toxin in Biological Materials by Gas
8
9 893 Chromatography Isotope Ratio Mass Spectrometry. *Analytical Chemistry* 87, 11732–
10
11 894 11738. <https://doi.org/10.1021/acs.analchem.5b02918>
12
- 13 895 Mason, R.P., Fitzgerald, W.F., 1990. Alkylmercury species in the equatorial Pacific. *Nature* 347,
14
15 896 457–459. <https://doi.org/10.1038/347457a0>
- 16 897 Mason, R.P., Reinfelder, J.R., Morel, F.M.M., 1996. Uptake, Toxicity, and Trophic Transfer of
17
18 898 Mercury in a Coastal Diatom. *Environmental Science & Technology* 30, 1835–1845.
19
20 899 <https://doi.org/10.1021/es950373d>
21
- 22 900 Mason, R.P., 2021. Coastal Phytoplankton and Mercury Dynamics in Watersheds Along the U.S.
23
24 901 East Coast From New Jersey to Maine Assessed Using Particulate and Dissolved
25
26 902 Samples Collected in 2015 and 2016. Biological and Chemical Oceanography Data
27
28 903 Management Office (BCO-DMO).
- 29 904 Mason, R.P., Buckman, K.L., Seelen, E.A., Taylor, V.F., Chen, C.Y., 2023. An examination of
30
31 905 the factors influencing the bioaccumulation of methylmercury at the base of the
32
33 906 estuarine food web. *Science of The Total Environment* 886, 163996.
34
35 907 <https://doi.org/10.1016/j.scitotenv.2023.163996>
- 36 908 Maulvault, A.L., Custódio, A., Anacleto, P., Repolho, T., Pousão, P., Nunes, M.L., Diniz, M.,
37
38 909 Rosa, R., Marques, A., 2016. Bioaccumulation and elimination of mercury in juvenile
39
40 910 seabass (*Dicentrarchus labrax*) in a warmer environment. *Environmental Research* 149,
41
42 911 77–85. <https://doi.org/10.1016/j.envres.2016.04.035>
43
- 44 912 Médieu, A., Point, D., Itai, T., Angot, H., Buchanan, P.J., Allain, V., Fuller, L., Griffiths, S.,
45
46 913 Gillikin, D.P., Sonke, J.E., Heimbürger-Boavida, L.-E., Desgranges, M.-M., Menkes,
47
48 914 C.E., Madigan, D.J., Brosset, P., Gauthier, O., Tagliabue, A., Bopp, L., Verheyden, A.,
49
50 915 Lorrain, A., 2022. Evidence that Pacific tuna mercury levels are driven by marine
51
52 916 methylmercury production and anthropogenic inputs. *Proceedings of the National*
53
54 917 *Academy of Sciences* 119, e2113032119. <https://doi.org/10.1073/pnas.2113032119>
55
- 56 918 Monperrus, M., Tessier, E., Amouroux, D., Leynaert, A., Huonnic, P., Donard, O.F.X., 2007.
57
58 919 Mercury methylation, demethylation and reduction rates in coastal and marine surface
59
60 920 waters of the Mediterranean Sea. *Marine Chemistry* 107, 49–63.
61
62
63
64
65

- 921 <https://doi.org/10.1016/j.marchem.2007.01.018>
- 1
2 922 Morel, F.M.M., Kraepiel, A.M.L., Amyot, M., 1998. The Chemical Cycle and Bioaccumulation
3
4 923 of Mercury. *Annual Review of Ecology and Systematics* 29, 543–566.
5
6 924 <https://doi.org/10.1146/annurev.ecolsys.29.1.543>
- 7 925 Nfon, E., Cousins, I.T., Järvinen, O., Mukherjee, A.B., Verta, M., Broman, D., 2009.
8
9 926 Trophodynamics of mercury and other trace elements in a pelagic food chain from the
10
11 927 Baltic Sea. *Science of The Total Environment* 407, 6267–6274.
12
13 928 <https://doi.org/10.1016/j.scitotenv.2009.08.032>
- 14 929 Outridge, P.M., Mason, R.P., Wang, F., Guerrero, S., Heimbürger-Boavida, L.E., 2018. Updated
15
16 930 Global and Oceanic Mercury Budgets for the United Nations Global Mercury
17
18 931 Assessment 2018. *Environmental Science & Technology* 52, 11466–11477.
19
20 932 <https://doi.org/10.1021/acs.est.8b01246>
- 21
22 933 Petrova, M.V., Ourgaud, M., Boavida, J.R.H., Dufour, A., Tesán Onrubia, J.A., Lozingot, A.,
23
24 934 Heimbürger-Boavida, L.-E., 2020. Human mercury exposure levels and fish
25
26 935 consumption at the French Riviera. *Chemosphere* 258, 127232.
27
28 936 <https://doi.org/10.1016/j.chemosphere.2020.127232>
- 29 937 Pućko, M., Burt, A., Walkusz, W., Wang, F., Macdonald, R.W., Rysgaard, S., Barber, D.G.,
30
31 938 Tremblay, J.-é., Stern, G.A., 2014. Transformation of Mercury at the Bottom of the
32
33 939 Arctic Food Web: An Overlooked Puzzle in the Mercury Exposure Narrative.
34
35 940 *Environmental Science & Technology* 48, 7280–7288.
36
37 941 <https://doi.org/10.1021/es404851b>
- 38 942 Rau, G., Teyssie, J., Rassoulzadegan, F., Fowler, S., 1990. C-13/C-12 and N-15/N-14 variations
39
40 943 among size-fractionated marine particles - implications for their origin and trophic
41
42 944 relationships. *Marine Ecology Progress Series* 7.
- 43
44 945 Ravichandran, M., 2004. Interactions between mercury and dissolved organic matter—a review.
45
46 946 *Chemosphere* 55, 319–331. <https://doi.org/10.1016/j.chemosphere.2003.11.011>
- 47 947 R Core Team, 2013. R: A Language and Environment for Statistical Computing. R Foundation
48
49 948 for Statistical Computing, Vienna.
- 50
51 949 Remen, M., Nederlof, M.A.J., Folkedal, O., Thorsheim, G., Sitjà-Bobadilla, A., Pérez-Sánchez,
52
53 950 J., Oppedal, F., Olsen, R.E., 2015. Effect of temperature on the metabolism, behaviour
54
55 951 and oxygen requirements of *Sparus aurata*. *Aquaculture Environment Interactions* 7,
56
57 952 115–123. <https://doi.org/10.3354/aei00141>
- 58 953 Rolff, C., 2000. Seasonal variation in $\delta^{13}\text{C}$ and $\delta^{15}\text{N}$ of size-fractionated plankton at a coastal

- 954 station in the northern Baltic proper. *Marine Ecology Progress Series* 203, 47–65.
1 955 <https://doi.org/10.3354/meps203047>
2
3 956 Rosati, G., Solidoro, C., Canu, D., 2020. Mercury dynamics in a changing coastal area over
4 industrial and postindustrial phases: Lessons from the Venice Lagoon. *Science of The*
5 957 *Total Environment* 743, 140586. <https://doi.org/10.1016/j.scitotenv.2020.140586>
6 958
7 959 Rosati, G., Canu, D., Lazzari, P., Solidoro, C., 2022. Assessing the spatial and temporal
8 variability of methylmercury biogeochemistry and bioaccumulation in the
9 960 Mediterranean Sea with a coupled 3D model. *Biogeosciences* 19, 3663–3682.
10 961 <https://doi.org/10.5194/bg-19-3663-2022>
11 962
12 963 Schartup, A.T., Qureshi, A., Dassuncao, C., Thackray, C.P., Harding, G., Sunderland, E.M.,
13 964 2018. A Model for Methylmercury Uptake and Trophic Transfer by Marine Plankton.
14 965 *Environmental Science & Technology* 52, 654–662.
15 966 <https://doi.org/10.1021/acs.est.7b03821>
16 967 Sharif, A., Monperrus, M., Tessier, E., Amouroux, D., 2013. Determination of methyl mercury
17 968 and inorganic mercury in natural waters at the pgL⁻¹ level: Intercomparison between
18 969 PT-GC-Pyr-AFS and GC-ICP-MS using Ethylation or Propylation derivatization. *E3S*
19 970 *Web of Conferences* 1, 09001. <https://doi.org/10.1051/e3sconf/20130109001>
20 971 Silva, A., Carrera, P., Massé, J., Uriarte, A., Santos, M.B., Oliveira, P.B., Soares, E., Porteiro, C.,
21 972 Stratoudakis, Y., 2008. Geographic variability of sardine growth across the northeastern
22 973 Atlantic and the Mediterranean Sea. *Fisheries Research* 90, 56–69.
23 974 <https://doi.org/10.1016/j.fishres.2007.09.011>
24 975 Sommer, U., Stibor, H., Katechakis, A., Sommer, F., Hansen, T., 2002. Pelagic food web
25 976 configurations at different levels of nutrient richness and their implications for the ratio
26 977 fish production:primary production, in: Vadstein, O., Olsen, Y. (Eds.), *Sustainable*
27 978 *Increase of Marine Harvesting: Fundamental Mechanisms and New Concepts*. Springer
28 979 Netherlands, Dordrecht, pp. 11–20. https://doi.org/10.1007/978-94-017-3190-4_2
29 980 Søreide, J.E., Hop, H., Carroll, M.L., Falk-Petersen, S., Hegseth, E.N., 2006. Seasonal food web
30 981 structures and sympagic–pelagic coupling in the European Arctic revealed by stable
31 982 isotopes and a two-source food web model. *Progress in Oceanography* 71, 59–87.
32 983 <https://doi.org/10.1016/j.pocean.2006.06.001>
33 984 Stern, G.A., Macdonald, R.W., 2005. Biogeographic Provinces of Total and Methyl Mercury in
34 985 Zooplankton and Fish from the Beaufort and Chukchi Seas: Results from the SHEBA
35 986 Drift. *Environmental Science & Technology* 39, 4707–4713.

- 987 <https://doi.org/10.1021/es0482278>
- 1
2 988 Storelli, M.M., Marcotrigiano, G.O., 2001. Total mercury levels in muscle tissue of swordfish
3
4 989 (*Xiphias gladius*) and bluefin tuna (*Thunnus thynnus*) from the Mediterranean Sea
5
6 990 (Italy). *Journal of Food Protection* 64, 1058–1061. [https://doi.org/10.4315/0362-028x-](https://doi.org/10.4315/0362-028x-64.7.1058)
7 991 [64.7.1058](https://doi.org/10.4315/0362-028x-64.7.1058)
- 8
9 992 Sunderland, E.M., Krabbenhoft, D.P., Moreau, J.W., Strode, S.A., Landing, W.M., 2009.
10
11 993 Mercury sources, distribution, and bioavailability in the North Pacific Ocean: Insights
12
13 994 from data and models. *Global Biogeochemical Cycles* 23.
14
15 995 <https://doi.org/10.1029/2008GB003425>
- 16 996 Tedetti, M., Tronczynski, J., 2019. HIPPOCAMPE Cruise. RV Antea. [https://doi.org/](https://doi.org/10.17600/18000900)
17
18 997 [10.17600/18000900](https://doi.org/10.17600/18000900).
- 19
20 998 Tedetti, M., Tronczynski, J., Carlotti, F., Pagano, M., Ismail, S.B., Sammari, C., Hassen, M.B.,
21
22 999 Desboeufs, K., Poindron, C., Chifflet, S., Zouari, A.B., Abdennadher, M., Amri, S.,
23
24 1000 Bănaru, D., Abdallah, L.B., Bhairy, N., Boudriga, I., Bourin, A., Brach-Papa, C., Briant,
25
26 1001 N., Cabrol, L., Chevalier, C., Chouba, L., Coudray, S., Yahia, M.N.D., de Garidel-
27
28 1002 Thoron, T., Dufour, A., Dutay, J.-C., Espinasse, B., Fierro-González, P., Fornier, M.,
29
30 1003 Garcia, N., Giner, F., Guigue, C., Guilloux, L., Hamza, A., Heimbürger-Boavida, L.-E.,
31
32 1004 Jacquet, S., Knoery, J., Lajnef, R., Belkahia, N.M., Malengros, D., Martinot, P.L.,
33
34 1005 Bosse, A., Mazur, J.-C., Meddeb, M., Misson, B., Pringault, O., Quéméneur, M.,
35
36 1006 Radakovitch, O., Raimbault, P., Ravel, C., Rossi, V., Rwawi, C., Hlaili, A.S., Tesán-
37
38 1007 Onrubia, J.A., Thomas, B., Thyssen, M., Zaaboub, N., Garnier, C., 2023. Contamination
39
40 1008 of planktonic food webs in the Mediterranean Sea: Setting the frame for the MERITE-
41
42 1009 HIPPOCAMPE oceanographic cruise (spring 2019). *Marine Pollution Bulletin* 189,
43
44 1010 114765. <https://doi.org/10.1016/j.marpolbul.2023.114765>
- 45
46 1011 Tesán-Onrubia, J.A., Petrova, M.V., Puigcorbé, V., Black, E.E., Valk, O., Dufour, A., Hamelin,
47
48 1012 B., Buessler, K.O., Masqué, P., Le Moigne, F.A.C., Sonke, J.E., Rutgers van der Loeff,
49
50 1013 M., Heimbürger-Boavida, L.-E., 2020. Mercury Export Flux in the Arctic Ocean
51
52 1014 Estimated from 234 Th/ 238 U Disequilibria. *ACS Earth and Space Chemistry*.
53
54 1015 <https://doi.org/10.1021/acsearthspacechem.0c00055>
- 55
56 1016 Tesán-Onrubia, J.A., Tedetti, M., Carlotti, F., Tenaille, M., Guilloux, L., Pagano, M., Lebreton,
57
58 1017 B., Guillou, G., Fierro-González, P., Guigue, C., Chifflet, S., Garcia, T., Boudriga, I.,
59
60 1018 Belhassen, M., Zouari, A.B., Bănaru, D., 2023. Spatial variations of biochemical
61
62 1019 content and stable isotope ratios of size-fractionated plankton in the Mediterranean Sea

- 1020 (MERITE-HIPPOCAMPE campaign). *Marine Pollution Bulletin* 189, 114787.
1
2 1021 <https://doi.org/10.1016/j.marpolbul.2023.114787>
3
4 1022 Tessier, E., Garnier, C., Mullot, J.-U., Lenoble, V., Arnaud, M., Raynaud, M., Mounier, S., 2011.
5 1023 Study of the spatial and historical distribution of sediment inorganic contamination in
6
7 1024 the Toulon bay (France). *Marine Pollution Bulletin* 62, 2075–2086.
8
9 1025 <https://doi.org/10.1016/j.marpolbul.2011.07.022>
10
11 1026 Tseng, C.-M., Ang, S.-J., Chen, Y.-S., Shiao, J.-C., Lamborg, C.H., He, X., Reinfelder, J.R.,
12
13 1027 2021. Bluefin tuna reveal global patterns of mercury pollution and bioavailability in the
14
15 1028 world's oceans. *Proceedings of the National Academy of Sciences* 118.
16 1029 <https://doi.org/10.1073/pnas.2111205118>
17
18 1030 Tsui, M.T.K., Wang, W.-X., 2004. Uptake and elimination routes of inorganic mercury and
19
20 1031 methylmercury in *Daphnia magna*. *Environmental Science & Technology* 38, 808–816.
21
22 1032 <https://doi.org/10.1021/es034638x>
23
24 1033 UN-Environment. Global Mercury Assessment 2018. United Nation Environmental Programme,
25
26 1034 Chemicals and Health Branch, Programme Chemicals and Health Branch Geneva
27
28 1035 Switzerland, 2019; [www.unenvironment.org/resources/publication/global-](http://www.unenvironment.org/resources/publication/global-mercuryassessment-2018)
29 1036 [mercuryassessment-2018](http://www.unenvironment.org/resources/publication/global-mercuryassessment-2018).
30
31 1037 Villar, E., Cabrol, L., Heimbürger-Boavida, L.-E., 2020. Widespread microbial mercury
32
33 1038 methylation genes in the global ocean. *Environmental Microbiology Reports* 12, 277–
34
35 1039 287. <https://doi.org/10.1111/1758-2229.12829>
36
37 1040 Wang, F., Outridge, P.M., Feng, X., Meng, B., Heimbürger-Boavida, L.-E., Mason, R.P., 2019.
38 1041 How closely do mercury trends in fish and other aquatic wildlife track those in the
39
40 1042 atmosphere? – Implications for evaluating the effectiveness of the Minamata
41
42 1043 Convention. *Science of The Total Environment* 674, 58–70.
43
44 1044 <https://doi.org/10.1016/j.scitotenv.2019.04.101>
45
46 1045 Wu, P., Dutkiewicz, S., Monier, E., Zhang, Y., 2021. Bottom-Heavy Trophic Pyramids Impair
47 1046 Methylmercury Biomagnification in the Marine Plankton Ecosystems. *Environmental*
48
49 1047 *Science & Technology*. 55, 15476–15483. <https://doi.org/10.1021/acs.est.1c04083>
50
51 1048 Wu, Y., Wang, W.-X., 2011. Accumulation, subcellular distribution and toxicity of inorganic
52
53 1049 mercury and methylmercury in marine phytoplankton. *Environmental Pollution*,
54
55 1050 Nitrogen Deposition, Critical Loads and Biodiversity 159, 3097–3105.
56
57 1051 <https://doi.org/10.1016/j.envpol.2011.04.012>
58
59 1052 Yoon, S.-J., Diener, L.M., Bloom, P.R., Nater, E.A., Bleam, W.F., 2005. X-ray absorption
60
61
62
63
64
65

1053 studies of CH₃Hg⁺-binding sites in humic substances. *Geochimica et Cosmochimica*
1 1054 *Acta* 69, 1111–1121. <https://doi.org/10.1016/j.gca.2004.07.036>
2
3 1055 Zhang, Y., Jaeglé L., Thompson L., 2014. Natural biogeochemical cycle of mercury in a global
4
5 1056 three-dimensional ocean tracer model. *Global Biogeochemical Cycles* 28, 553–570.
6
7 1057 <https://doi.org/10.1002/2014GB004814>
8
9 1058 Zhang, Y., Soerensen, A.L., Schartup, A.T., Sunderland, E.M., 2020. A global model for
10
11 1059 methylmercury formation and uptake at the base of marine food webs. *Global*
12
13 1060 *Biogeochemical Cycles*. <https://doi.org/10.1029/2019GB006348>
14
15 1061
16
17 1062
18
19 1063
20
21 1064
22
23 1065
24
25 1066
26
27 1067
28
29 1068
30
31 1069
32
33 1070
34
35 1071
36
37 1072
38
39 1073
40
41 1074
42
43 1075
44
45 1076
46
47 1077
48
49 1078
50
51 1079
52
53 1080
54
55 1081
56
57 1082
58
59 1083
60
61
62
63
64
65

Figure captions

Figure 1: Location of the ten sampling stations of the MERITE-HIPPOCAMPE cruise in the Mediterranean Sea (April-Mai 2019).

Figure 2: Boxplot of the concentrations of A) THg, B) MMHg (ng g⁻¹ dw) and C) %MMHg in the different plankton size-fractions (fractions between 0.7 and 20 µm (green scale) and >60 µm (red scale) for all stations combined. H = Kruskal–Wallis nonparametric test and the associated p-value for the respective Hg species (H = 24, p < 0.0001; H = 36, p < 0.0001 and H = 30, p < 0.0001, respectively). The mean and median values are represented by a cross and a horizontal line, respectively, and the box length is defined as the interquartile range. The minimum and maximum values are represented by whiskers. Mean values with different post-hoc letters are significantly different (p < 0.05).

Figure 3: Logarithm of THg (A) and MMHg (B) concentrations in function of δ¹⁵N (‰) in the different phyto- (green dots) and zooplankton (red dots) size-fractions. The linear regression curve with its equation and the R-square are indicated.

Figure 4: Transfer efficiency between phytoplankton (0.7 to 20 µm fractions) and zooplankton (>60 µm fractions) amounts of THg (A) and MMHg (B) (in pg m⁻³) by station. Yellow, orange and red isolines represent transfer efficiencies of 1, 5 and 10% for THg and 10, 50 and 100% for MMHg, respectively.

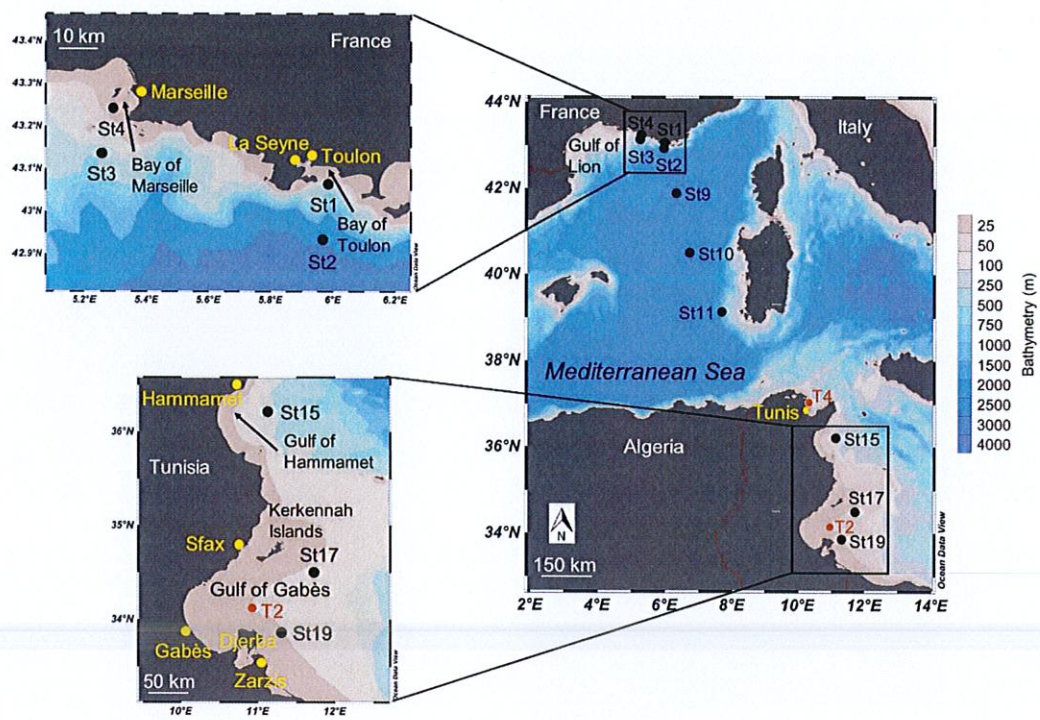
Figure 5: Box plots of A) THg (yellow) and B) MMHg (red) (in ng g⁻¹ dw) concentrations measured in the 60 to 1000 µm zooplankton size-fractions by station. The mean and median values are represented by a cross and a horizontal line, respectively, and the box length is defined as the interquartile range.

Figure 6: Trophic magnification factors of THg (TMF_{THg}, in yellow) and MMHg (TMF_{MMHg} in red) at the different stations. >1 values indicated biomagnification, while <1 indicated bioreduction.

1114 **Figures**

1115

2
3
4
5
6
7
8
9
10
11
12
13
14
15
16
17
18
19
20
21
22
23
24
25
26
271116



1117 **Figure 1**

28
29
30
31
32
33
34
35
36
37
38
39
40
41
42
43
44
45
46
47
48
49
50
51
52
53
54
55
56
57
58
59
60
61
62
63
64
65

15
16
17
18
19
20
21
22
23
24
25
26
27
28
29
30
31
32
33
34
35
36
37
38
39
40
41
42
43
44
45
46
47
48
49
50
51
52
53
54
55
56
57
58
59
60
61
62
63
64
65

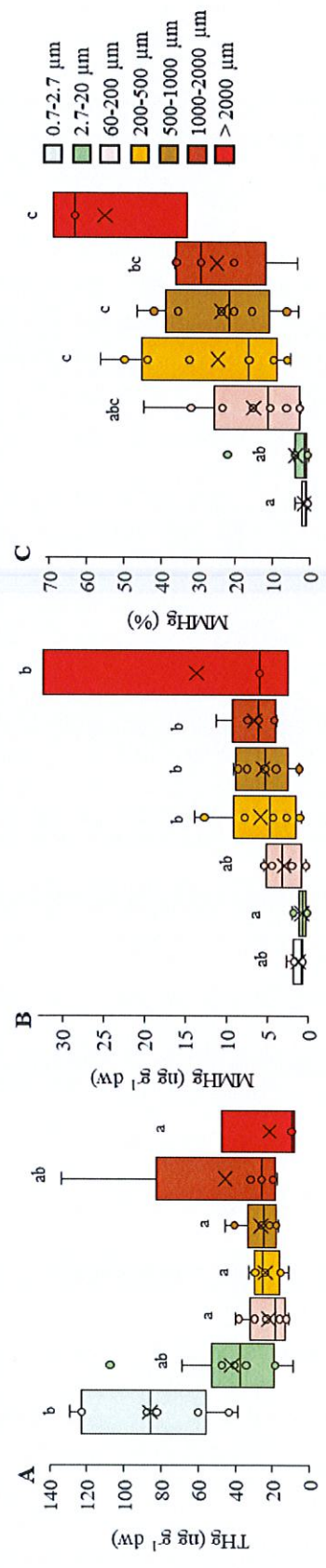
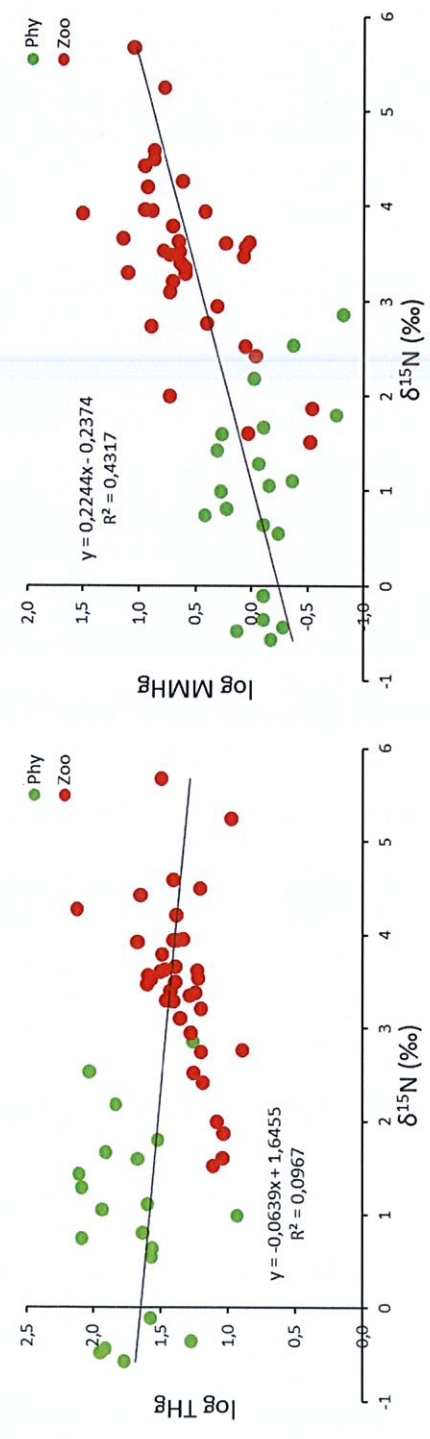


Figure 2



1118
1119
1120
1121
1122
1123
1124
1125
1126

15
 16
 17
 18
 19
 20
 21
 22
 23
 24
 25
 26
 27
 28
 29
 30
 31
 32
 33
 34
 35
 36
 37
 38
 39
 40
 41
 42
 43
 44
 45
 46
 47
 48
 49
 50
 51
 52
 53
 54
 55
 56
 57
 58
 59
 60
 61
 62
 63
 64
 65

Figure 3

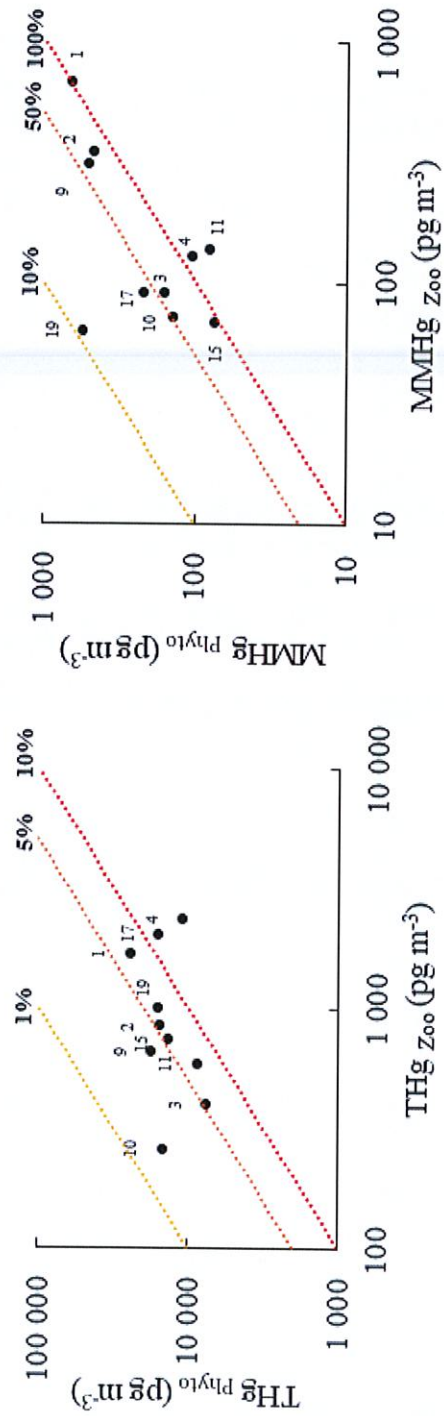


Figure 4

THg_{Zoo} (pg m⁻³)

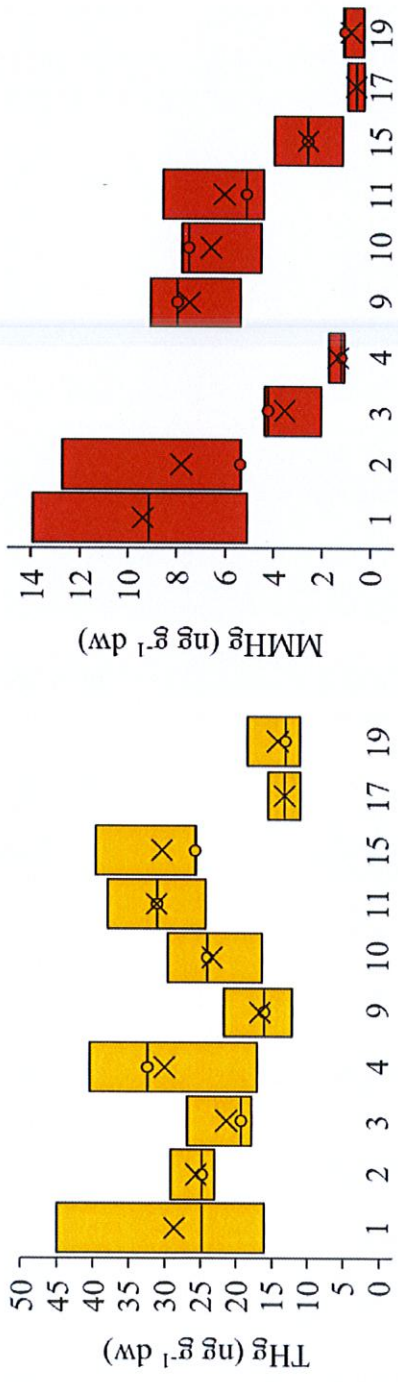


Figure 5

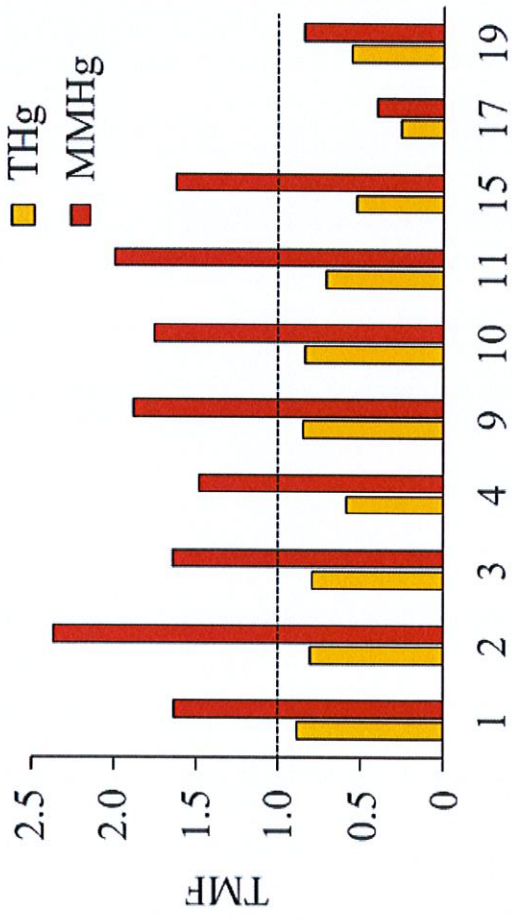
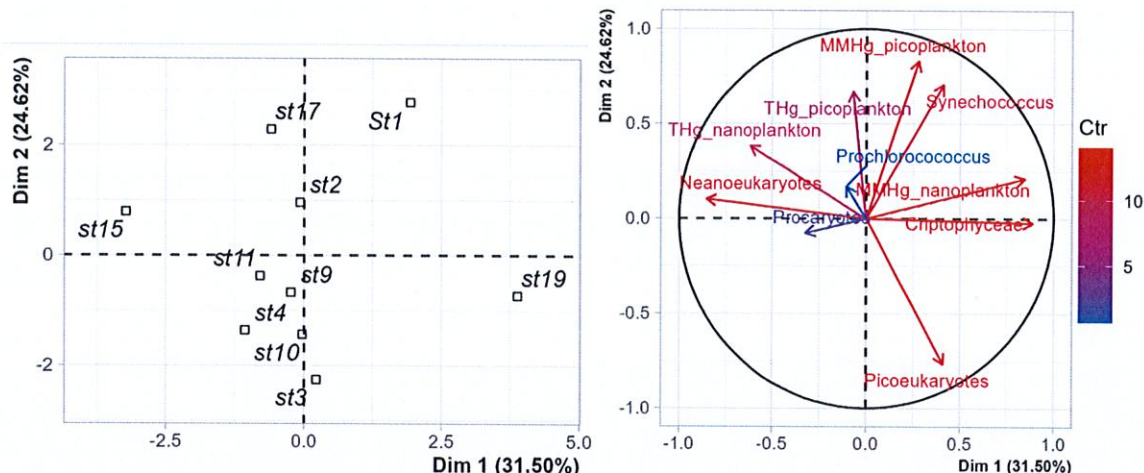


Figure 6

1145 Supplementary information



1146
 1147 **Figure S1:** Principal component analysis of the phytoplankton composition (*Synechococcus* spp.,
 1148 *Prochlorococcus* spp., picoekaryotes, nanoekaryotes and cryptophyceae), THg and MMHg in the 0.7–2.7 and
 1149 2.7–20 μm size-fractions by station. Color gradient indicates the contribution of the variables from blue for low
 1150 contribution to red for high contribution.

1
 2
 3
 4
 5
 6
 7
 8
 9
 10
 11
 12
 13
 14
 15
 16
 17
 18
 19
 20
 21
 22
 23
 24
 25
 26
 27
 28
 29
 30
 31
 32
 33
 34
 35
 36
 37
 38
 39
 40
 41
 42
 43
 44
 45
 46
 47
 48
 49
 50
 51
 52
 53
 54
 55
 56
 57
 58
 59
 60
 61
 62
 63
 64
 65

1
2
3
4
5
6
7
8
9
10
11
12
13
14
15
16
17
18
19
20
21
22
23
24
25
26
27
28
29
30
31
32
33
34
35
36
37
38
39
40
41
42
43
44
45
46
47
48
49
50
51
52
53
54
55
56
57
58
59
60
61
62
63
64
65

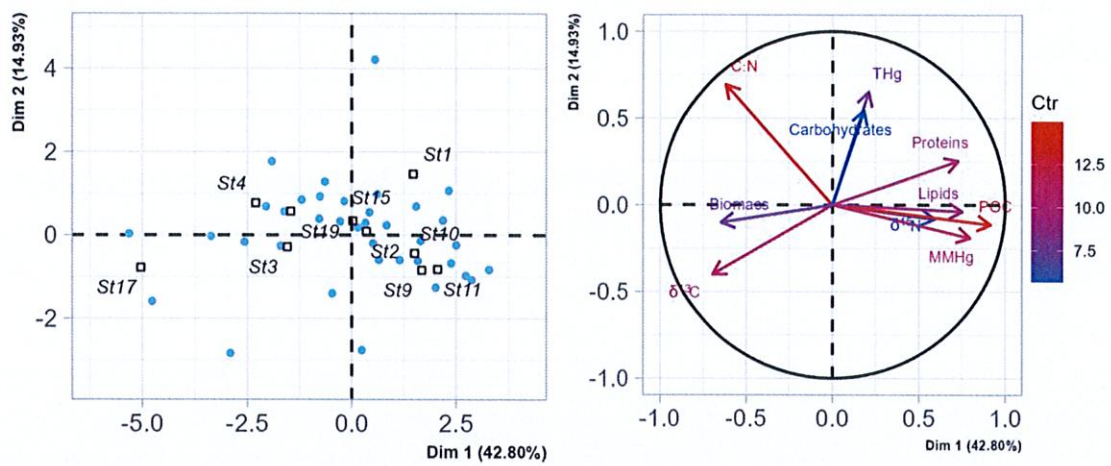


Figure S2: Principal component analysis of the biochemical variables (zooplankton biomass, $\delta^{13}\text{C}$, $\delta^{15}\text{N}$, C/N, POC, proteins, carbohydrates and lipids), THg and MMHg in zooplankton (60 to 1000 μm fractions) by station. Color gradient indicates the contribution of the variables from blue for low contribution to red for high contribution.

Table S1. Main characteristics of the ten sampling stations of the MERITE-HIPPOCAMPE cruise (13 April–14 May 2019) aboard the R/V *Anitea* along a north-south transect in the Mediterranean Sea. The environmental conditions in these stations were detailed in Tedetti et al. (2023).

Station	Location	Latitude (N)	Longitude (E)	Bottom depth (m)	McLane sampling depth (m)	MultiNet sampling depth (m)
St1	Bay of Toulon (north)	43° 03.819'	5° 59.080'	91	20	20
St2	Toulon - Aniharcs (north)	42° 56.020'	5° 58.041'	1770	25	34
St3	Marsaille - Julio (north)	43° 08.150'	5° 15.280'	95	55	58
St4	Bay of Marsaille (north)	43° 14.500'	5° 17.500'	58	31	35
St9	North Balearic Front (offshore)	41° 53.508'	6° 19.998'	2575	20	20
St10	North Balearic Front (offshore)	40° 18.632'	7° 14.753'	2791	50	30
St11	North Balearic Front (offshore)	39° 07.998'	7° 41.010'	1378	40	30
St15	Gulf of Hammamet (south)	36° 12.883'	11° 07.641'	100	40	60
St17	Gulf of Gabès (south)	34° 30.113'	11° 43.573'	50	40	40